AD-A044 688 CONTROL DATA CORP MELVILLE N Y TRG DIV F/G 20/1
PURVIS II SECOND DATA ANALYSIS REPORT,(U)
MAY 67 D CHASE
UNCLASSIFIED TRG-023-TM-67-19 NOBSR-93023 NL

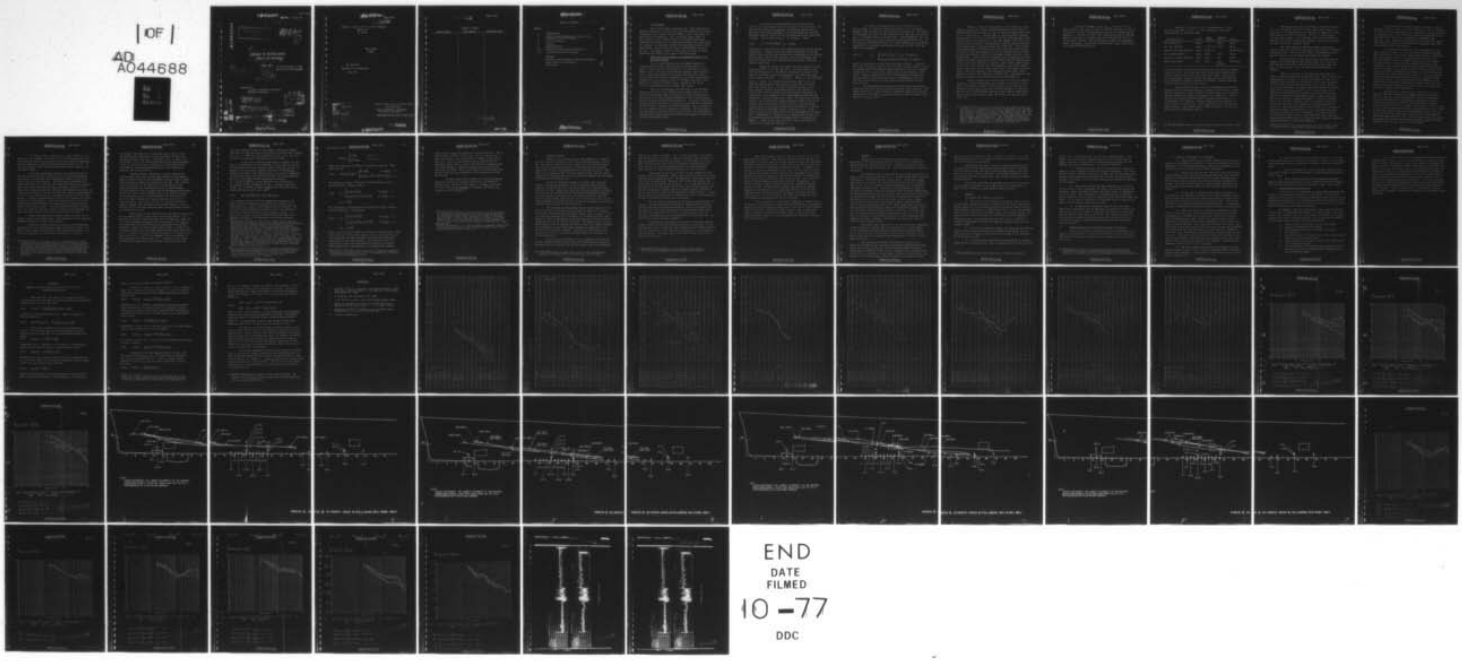

END
DATE FILMED
10-77
DDC

CONFIDENTIAL

B067-47022

MOST Project-4

UNCLASSIFIED TRG Div
Control Data Grp

(1)

B 5.

(6)

PURVIS II SECOND DATA ANALYSIS REPORT(U)

(11) MAY 1967

This Document Consists of 53 Pages
No. 2 of 5 Copies Series O

(10) D. Chase

(12) 69 p.

SUBMITTED TO:

U. S. NAVY ELECTRONICS LABORATORY
SAN DIEGO, CALIFORNIA

CONTRACT NO.:

(15) NObsr-93023

REPORT NO.:

(14) TRG-023-TM-67-19

UNCLASSIFIED

353 425

CONFIDENTIAL

~~CONFIDENTIAL~~

B067-47022

UNCLASSIFIED

PURVIS II SECOND DATA ANALYSIS REPORT (U)

(TM-67-19)

D. Chase

WAD 13B067

47022

TRG DIVISION

CONTROL DATA CORPORATION, S.D., Ca.

May 1967

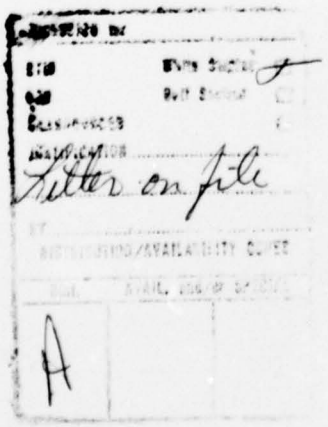

Produced Under Contract NObsr 93023

for Code 2110

NAVY ELECTRONICS LABORATORY
San Diego, California

CONFORMAL/PLANAR ARRAY SONAR SYSTE

UNCLASSIFIED

~~CONFIDENTIAL~~

RECORD OF CHANGE

CHANGE NUMBER	PAGE NUMBER	EFFECTIVE DATE

TABLE OF CONTENTS

Partial contents:

1. INTRODUCTION

The present report represents the second stage of the first-cut analysis of acoustic data from the PURVIS II sea tests, containing some reference also to PURVIS I data. The report is presented as an updating of the first-stage report (Ref. 4) with regard to those aspects which in the interim have been substantially illuminated or modified by further data processing or analysis. An integrated report dealing comprehensively with both PURVIS I and II first-cut data is scheduled for the end of June. The present report contains also a summary of recommendations for PURVIS II second-cut data processing.

2. NOISE ON FLUSH ELEMENTS; ITS SOURCES AND SCALING IN DISTINCT DOMAINS

It is a prime objective in the PURVIS analysis to identify reliably the principal sources and dependences of noise on flush elements with reference, in particular, to frequency, speed, aft and circumferential position, and transducer size. Such understanding is especially desired with respect to the large 5"-D elements of PURVIS II; we pursue this analysis further here with regard to those 5" elements presumably least affected by bubble or surface noise, notably the HF and LF elements, with emphasis on the higher ship speeds.

Since it is indicated that TBL noise is the dominant component for even the 5" elements at the higher speeds in at least a considerable range of frequency, we again view results by reference to a plot nondimensionalized in some roughly appropriate way based on TBL-related parameters. Possible scaling laws for TBL pressure spectra are summarized in the Appendix; depending on the domain of frequency and other variables, one or another of these is expected to have approximate validity. To each scaling law, provided it expresses the spectrum in terms of a function of a single dimensionless frequency variable, corresponds a particular type of dimensionless plot.

We start here with presentation of noise data in terms of the dimensionless plot used recently by Foxwell (Ref. 3); for present convenience, however, we modify the dimensionless spectrum from $P(\omega/2\pi)/\rho^2 R_o v_*^4 U_\infty^{-1}$ to $P(\omega/2\pi)/\rho^2 R_o U_\infty^3$ (see Appendix, Eq.(A10)) without concern for the weak Reynolds-number dependence of v_*/U_∞. Thus we plot $10\log\pi_o'$ vs. $10\log\Omega_o$, where

$$(2\text{-}1) \qquad \pi_o' = P(\omega/2\pi)\rho^2 R_o U_\infty^3, \quad \Omega_o = \omega R_o/U_\infty,$$

and $P(\omega/2\pi)$ is the noise-pressure spectrum measured by the element in question. Though we may well expect departures of the TBL pressure spectrum from the scaling law corresponding to coalescence on this type of plot, this type does seem most convenient and least misleading for basic presentation of results, and worth further evaluation.

Figure 2-1 shows such a plot for noise spectra measured by HF-7 and LF-1 at 10, 20, and 30 kt. For fixed element size and fixed distance aft, the degree coalescence of plots of this type for different speeds is necessarily very nearly the same as on a plot of $10\log\pi_1$ vs. $10\log\Omega_1$, where $\pi_1 = P(\omega/2\pi)/\rho^2\delta_* U_\infty^3$ and $\Omega_1 = \omega\delta_*/U_\infty$. As in the previous report (Ref. 4), we see that the coalescence for HF-7 and LF-1 separately is fairly close for 20 and 30 kt. At 10 kt especially in the case of LF-7, which is nearer the machinery spaces, the curves are higher; this result is expected if the relative importance of an acoustic noise component, less speed-dependent than the TBL component, is great at this lower speed. The curves for the two elements (at 20 and 30 kt) likewise nearly coalesce with one an another; this circumstance reflects the fact, also noted previously (Ref. 4), that the measured noise on elements of the HF and LF arrays at the higher speeds is similar, i.e., in the domain of measurement the noise is nearly independent of distance aft. Independence of distance aft is observed also in the case of the noise spectra on 1/8" D elements (FS-1's) measured in PURVIS I. These results are consistent, then, with Foxwell's scaling law, though not uniquely so.

The degree of coalescence of the FS-1 spectra on the (Ω_o,π_o) plot for different speeds and distances aft, as given by elements 1638 and 1628, is shown explicitly in Fig. 2-3. The degree of conformance (except for the leveling of the 1628 spectrum at 20 kt due to a non-TBL source) is notably good. Correspondingly, the coalescence on the (Ω_1,π_1) plot is poor for different distances aft. In the latter connection we define a π_1' which modifies π_1 by including an asymptotic area-correction factor in accord with Eqs. (A4) and (A8) of the Appendix:

$$(2\text{-}1.1) \qquad \pi_1' = \begin{cases} P(\omega/2\pi/\rho^2\delta_*U_\infty^2 \ (\equiv \pi_1) \text{ if } \omega R_o/U_\infty \ll 1 \\ (\omega R_o/\eta U_\infty)^2 P(\omega/2\pi)/P^2\delta_*U_\infty^3 \text{ if } \omega R_o/U_\infty \gg 1, \end{cases}$$

where ηU_∞ represents an effective convection velocity. A plot of this (Ω_1,π_1') type is shown in Fig. 2-5 where we have taken η to have a constant value 0.71 and have joined the curves for the two ranges defined in (2-1.1) near their intersection by an arbitrary smooth curve. Curves B and C for the FS-1's at different distances aft diverge greatly, relative to Fig. 2-3, corresponding to the fact that the measured noise does not decrease with distance aft nor hence with δ_*.

We may similarly compare with the FS-1 spectra and among themselves the noise spectra measured by Franz on the Albacore. The Franz results for a given element at different speeds will coalesce moderately well on the (Ω_o,π_o) plot, since, as shown by Franz, they did on the (Ω_1,π_1) plot.

In Fig 2-4 we see a comparison at 20 kt among the Franz elements at the 6.2%, 10.5%, and 22.8% distances aft and the FS-1 element 1638*; the distances aft for the four are respectively 12.4, 21, 45.6, and 41.6 ft. Element 1638, as noted in earlier reports, measures noise from ~2 to 9 db lower than the 22.8% Albacore element at nearly the same distance aft. For the average of the FS-1's at this sea chest, moreover, the difference would be slightly greater, since 1638 measures slightly higher noise than most. In the range of frequency above 10 $\log\Omega_o \simeq 2$, where the slopes are rather steep, a few db of this difference may be due to attribution of too large an effective diameter (0.11") to the Franz element relative to the FS-1(0.125"). Also, the FS-1 was mounted in a fiberglass sea-chest window, which may constitute a softer baffle than the superstructure in which the Franz element was mounted. This effect could account at most for a 6 db difference, corresponding to the former baffle being transparent and the latter rigid, and at the higher values of $\omega R_o/U_\infty$, where the elements, with reference to TBL noise, create their own baffles, the difference would be less. Nevertheless, the agreement between these elements seems not unsatisfactory.

When we compare the results in Fig. 2-4 for the Albacore elements at different distances aft, however, we see poor coalescence, in contrast to Fig. 2-3 for the FS-1's. We view the comparisons on the ($\Omega_1 \Pi_1'$) plot [Eq. (2-1.1)] in Figs. 2-5 and 2-5A. The spectra for the Albacore elements do not coalesce appreciably better on this type of plot (Fig. 5A) than on the (Ω_o, Π_o') plot (Fig. 2-4).

* In Figs. 2-5 and 2-5A we have assumed for the Albacore plots not the values of δ_* obtained by Franz by integration of the measured mean velocity profiles but rather those computed by the same formula used in constructing the Purvis dimensionless plots (Ref. 4, Eq. (A1-6)). The latter computed δ_*'s are larger than the former by a roughly constant factor 1.4. The comparison between the Purvis and Albacore elements has thus been made on a consistent basis. This discrepancy in δ_*, however, requires investigation with regard to continued use of Eq. (A1-6) of Ref. 4.

Though the evidence for the (Ω_o,π_o') type of scaling law relative to the (Ω_1,π_1') type is thus not flawless, the FS-1's of Purvis I, as well as more diverse results to be presented, do support it. We must note that this evidence for ($\Omega_o\pi_o$') scaling based on elements of a single size, as of the FS-1's, does not at all imply, however, that the variable $\omega\nu/v_*^2$ is not pertinent along with $\omega R_o/U_\infty$, as discussed further below, since $\omega\nu/v_*^2$ varies very weakly with distance aft.

Results of a variety of noise measurements are shown in the (Ω_o, π_o') form in Fig. 2-1. The measurements shown are identified in the following table.

Identification	Fluid	Diam $2R_o$ (in.)	Distance aft. ft.	Speed z
HF-3, PURVIS II	water	5	26.8	20 kt
43, USL, Albacore	water	1.5 to 2.9	34.8	20 kt
Foxwell, rotating cylinder	water	0.125 to 1		37,78 ft/sec
FS-1, 1638, PURVIS I	water	0.125	41.5	20 kt
10.5% pt., Franz, Albacore	water	0.11	21	20 kt
Bull, wind tunnel	air	0.03	(δ_* = 0.149")	329 ft/sec

In each instance of sea-test measurements, we have chosen to display curves for 20 kt, but results at other (sufficiently high*) speeds coalesce fairly well on this plot with those shown. Furthermore, as we have noted, results at other distances aft are available for the 5"D PURVIS II elements and the FS-1 PURVIS I elements and also coalesce fairly well with those shown.

Also shown in Figure 2-2 is the extrapolated form of TBL spectrum recently inferred (Ref. 3) to apply in the limit of a point element ($\omega R_o/U_\infty \to 0$), namely $a\rho^2 U_\infty^4 \omega^{-1}$ (in which again we are neglecting the variation of v_*/U_∞; see Appendix, Eq. (A5)), where the coefficient a is taken as determined by the Bull measurements, i.e., the straight line $10\log\pi_o' = 10\log a - 10\log\Omega_o$ is made tangent to the Bull curve in Figure 2-2. This conjectured form is expected to apply, however, only roughly where $\omega\nu/v_*^2 \ll 1$ and hence does not actually hold for arbitrarily high Ω_o.

* The USL results coalesce rather well even at 10 kt (see Fig. 2-1A).

The appropriate effective diameter of the USL Albacore element is uncertain within the limits shown, since the sensing area was 1.5" in diameter but was covered by a rubber boot 3/16" thick that was 2-7/8" in diameter. In Fig. 2-2 the diameter 1.5" has been assumed. It is possible also that the effective diameter of the Franz element was somewhat smaller than assumed, and that of the FS-1 slightly larger.

The curve drawn for Foxwell's results represents a visual average of results for two speeds and a number of different transducer sizes. The actual data show a considerable spread, but the average curve is smooth and fairly well defined.

We recall that if the spectrum for the Franz Albacore element at the 22.8% point were shown in Fig. 2-2 in place of that for the 10.5% point, the curve would fall much lower and more in line with the curves for the FS-1 and the Foxwell elements.

The noise spectra of both USL43 and HF-3 display a bend at which the (negative) slope decreases*. This occurs in the neighborhood of $10\log\Omega_o = 14$ in the case of HF-3 at 20 kt and slightly higher in the case of USL 43 at 20 kt; the transition is particularly abrupt and pronounced in the latter instance. Up to this break-point, the spectra for HF-3 and USL 43 coincide rather well on the (Ω_o, π'_o) plot. (If we assumed $2R_o = 2.9"$ instead of 1.5"for USL 43, we should move this curve downward and to the right by 2.8 logarithmic units.) Above this point the curve for HF-3 is appreciably higher. Toward the highest values of Ω_o for HF-3 ($10\log\Omega_o \geq 22$), at which no results for USL 43 are available, the spectrum turns decidedly downward once more. The Foxwell spectra do not exhibit such a pronounced flattening effect, though Foxwell in fact suggested that some decrease in slope does occur at $10\log\Omega_o \simeq 16$. These spectra lie still lower than on USL 43 above the break-point, and also lower than USL 43 and HF-3 in a range of lower Ω_o before approaching USL 43 again at still lower frequency.

*This transition is scarcely defined in the case of HF-7 shown in Fig. 2-1 but is discernible for most HF and LF elements.

We may attempt to understand these results as follows. We suppose that the noise spectra for HF-3 (i.e., the 5" elements) and USL 43 at the higher speeds are dominated by the TBL component at frequencies up to the break-points where the slope decreases. This break-point occurs at a frequency $\sim 0.8(U_\infty/20\text{kt})$ kHz ($10\log\Omega_o \simeq 14$). Above these break-points we tentatively suppose that the noise spectra are dominated by a component other than direct TBL pressure fluctuations.

If another noise source in fact predominates in this upper frequency range, it is, at any rate, one which increases with speed much as if it were a TBL pressure field, as shown for HF-7, for example, by Fig. 2-1 and for USL 43 by Fig. 2-1A. On this evidence alone, it would be most natural to suppose that this noise is due to (1) the acoustic field due to (a) radiation to the sensing element by flow-excited vibrations of the hull at more or less distant points, (b) flow-excited vibrations of the hull surrounding the element, and (2) the pressure field (with the same parallel wave number $K = \omega/c$ as a radiated acoustic field) associated with the effect of compressibility of the TBL itself. The former noise (1) would depend on the ship or other mechanical configuration, whereas the latter (2) would be invariant and universal when properly scaled with the pertinent boundary-layer parameters.

We must recall, however, the evidence of the cross-spectral densities of noise on neighboring HF elements (Ref. 4, Vol. I). The cross-spectral magnitudes ordinarily displayed a pronounced decrease in the frequency range up to ~2 kHz as speed increased from 0 to 20 kt, and a perceptible decrease also in the range from 2 to ~8 kHz. In particular, at 20 kt there is some substantial range of frequency extending well above 2 kHz in which the computed cross-spectral magnitude appears too low to be attributed to a radiated acoustic field, or generally a field with wave number $k \lesssim \omega/c$. In this connection we may refer, for example, to the planar isotropic magnitude $|J_o(\omega\zeta/c)|$ shown in Ref. 4, Vol. 1, Figs. 3.1.2-1, 2, and others.

Therefore, in some frequency range above 1 kHz, where we would like to attribute the noise on HF's to something other than the direct TBL noise, the evidence of the cross-spectral magnitudes seems to implicate a field with parallel wave numbers $K \gtrsim \omega/c$. If so, the acoustic fields (1a) and (2) mentioned above could not be the source sought.

As for the possibility (1b) that the pressure field is that associated with local bending waves in the hull surrounding the elements, we estimate the resonant wave length of this field in the case of the HF elements. The hull plate surrounding the horizontal row of this array is 1/4" thick and attached to a doubler plate 1/2" thick, bringing the total thickness of steel to 3/4". For a thin steel plate of this thickness water-loaded on one side, at 2 kHz, for example, we find the resonant wave number is approximately 5.2 ft^{-1}, i.e., only twice that for sound in water at the same frequency. At higher frequencies the ratio of the resonant wave number to that of sound decreases. Hence the shortest waves that may be appreciably excited locally, the resonant waves, are not greatly shorter than acoustic waves. For this reason and others, we doubt that the conjecture that this source of noise is most important in some wide range above 1 kHz is the one most worth pursuing.*

Another possible high-wavenumber source is noise due to bubbles close to the element face. This hypothesis is not presently supported, however, by other observations.

Possibly we should attach less weight to the indication provided by the low cross-spectral magnitudes discussed above. We suggest (but cannot explain) that in many instances computed cross-spectral magnitudes are rather lower than might be expected.

---

* We note a pair of limiting results regarding the noise field on an element due to baffle vibration. If the baffle impedance is infinite, this field obviously vanishes, and if the baffle is a pressure-release surface and the element vanishingly small, this field must exactly cancel the total driving pressure on the baffle (e.g., the sum of the TBL pressure and that due to radiation from acoustic sources through the water to the point question).

For example, the magnitude for adjacent pairs of LF elements in numerous cases decreases considerably from 0 to 10 kt over a broad frequency range (e.g., see Ref. 4, Vol. 1, Figs. 3.1.2 - 83 and 87). Yet it is clearly indicated by the speed dependence of the LF autospectra (e.g., see Fig. 2-1) that some non-TBL contribution, presumably machinery noise, still marginally dominates the noise at 10 kt.

Pending further indications, we still tentatively ascribe much of the noise on the large elements in the subject upper frequency range to speed-dependent acoustic noise of types enumerated above rather than directly to the TBL. This attribution is important for the objective of assessing the noise reduction possible by increasing the size of flush elements. As noted, however, this assessment may be configuration-dependent. At the same time we must note the noise on the recessed element G5 at 30 kt (Fig. 3-1) is substantially below that on the HF and LF elements through the range in question as well as at lower frequency. This result, if it is a reliable indication, tends to suggest that the noise on the flush elements is due to the TBL even in the high-frequency range, being therefore subject to reduction by a dome.

With regard to the contribution to the TBL noise spectrum due to compressibility of the medium (source (2) above), it is possible to advance a plausible form for its dependence (Ref. 6). In a certain regime of interest this contribution is thought to be of the order of $b(v_*/c)^2$ times the extrapolated form $\rho^2 v_*^4 \omega^{-1}$ supposed to apply to a point element when $\omega\nu/v_*^2 \ll 1$, where b is an unknown coefficient conceivably substantially larger than unity. If $b = 1$, however, the factor $(v_*/c)^2$ represents a subtraction of about 74 db for $U_\infty = 20$ kt; the straight line corresponding to this assumption is shown in Fig. 2-2. According to this figure b could not greatly exceed unity without conflicting with the

low noise spectrum on HF-3 at the highest frequency (10 kHz)*. If b does not greatly exceed unity, however, we would then conclude from Fig. 2-2 that this compressibility effect is not important for HF-3 at frequencies substantially below 10 kHz.

In the lower frequency range where we suppose the TBL noise to predominate for all elements, we have still to account for the decrease in noise spectra viewed on the (Ω_o, π_o') plot of Figure 2-2 as we proceed from HF-3 and USL 43 to the Foxwell elements and then to FS-1 (where however, the earlier comparison of the Franz elements with the FS-1's must also be considered). We recall first that the TBL dimensionless spectrum $\pi_o \equiv P(\omega/2\pi)/\rho^2 v_*^4 U_\infty^{-1} R_o$ can be expected to be a function of $\Omega_o \equiv \omega R_o/U_\infty$ alone, as proposed in Ref. 3, roughly only where $\omega\nu/v_*^2 \ll 1$; at higher $\omega\nu/v_*^2$ we encounter the so-called viscous cutoff and expect rather only that**

$$(2\text{-}2) \qquad P(\omega/2\pi)/\rho^2 v_*^4 U_\infty^{-1} R_o = H(\omega\nu/v_*^2, \omega R_o/U_\infty)$$

It is suggested, then, that the progressive lowering of the $(\Omega_o \pi_o')$ curves just mentioned may be due to a decrease of π_o' with increasing $\omega\nu/v_*^2$ at fixed $\omega R_o/U_\infty$ as R_o is decreased. We can explore this possibility explicitly if we are prepared to assume a definite dependence of H on $\omega R_o/U_\infty$ in (2-2). In particular, suppose, in accord with Eqs. (A3) and (A6) of the Appendix referring to the dependence of the high-wavenumber

*We point out that the acoustic noise on HF-3 due to TBL compressibility or radiative sources can nearly vanish, nevertheless, in a very narrow frequency band at still higher frequency. Consider an acoustic noise field propagating parallel to the plane containing the element. If the associated point pressure spectrum is $N(\omega)$, the average-pressure spectrum on the element is $N(\omega)[2J_1(\omega R_o/c)/(\omega R_o/c)]^2$, where c is the speed of sound. This quantity has its first zero at a frequency $\omega/2\pi = 0.61c/R_o$; for $2R_o = 5"$ and in water, this yields $\omega/2\pi \simeq 14.3$ kHz; in Figure 2-2, with reference to this R_o, the corresponding abscissa is $10\log\Omega_o = 27.4$. This cancellation of a parallel sound field by area-averaging is not displayed by the compressibility-noise line in Fig. 2-2; this line takes no account of area-averaging and can apply only where $\omega R_o/c \lesssim 1$.

**Past consideration of models for the convective contribution to the TBL pressure spectrum lead us to believe, pending renewed investigation, that dependence on $\omega\nu/v_*^2$ likely is important even at values much less than unity, perhaps where $\omega\nu/v_*^2 \gtrsim 0.1$ or 0.2 (cf. Ref. 3 and 7).

contribution, that CONFIDENTIAL

$$H(y,x) = \begin{cases} x^{-1}h(y) & \text{if } x \ll 1 \\ \eta^3 x^{-4} h(y) & \text{if } x \gg 1, \end{cases}$$

where ηU_∞ represents an effective convection velocity. Then (2-2) becomes

$$(2\text{-}3) \qquad P(\omega/2\pi)/\rho^2 v_*^4 \omega^{-1} = \begin{cases} h(\omega\nu/v_*^2) & \text{if } \omega R_o/U_\infty \ll 1 \\ (\omega R_o/\eta U_\infty)^{-3} h(\omega\nu/v_*^2) & \text{if } \omega R_o/U_\infty \gg 1. \end{cases}$$

We should then expect coalescence of measured curves if we plot $10\log\tilde{\pi}_2$ vs. $10\log\Omega_2$, where

$$(2\text{-}4) \qquad \tilde{\pi}_2 = \begin{cases} P(\omega/2\pi)/\rho^2 \nu v_*^2 & \text{if } \omega R_o/U_\infty \ll 1 \\ (\omega R_o/\eta U_\infty)^3 P(\omega/2\pi)/\rho^2 \nu v_*^2 & \text{if } \omega R_o/U_\infty \gg 1, \end{cases}$$

$$\Omega_2 = \omega\nu/v_*^2 .$$

For convenience, disregarding the variation of v_*/U_∞, we plot instead $10\log\pi_2'$ vs. $10\log\Omega_2'$, where

$$(2\text{-}5) \qquad \pi_2' = \begin{cases} P(\omega/2\pi)/\rho^2 \nu U_\infty^2 & \text{if } \omega R_o/U_\infty \ll 1 \\ (\omega R_o/\eta U_\infty)^3 P(\omega/2\pi)/\rho^2 \nu U_\infty^2 & \text{if } \omega R_o/U_\infty \gg 1, \end{cases}$$

$$\Omega_2' = \omega\nu/U_\infty^2 .$$

Such a plot is shown for HF-3 at 20 and 25 kt and for FS-1, 1638, at 20 and 30 kt in Fig. 2-6, where, in the case of the FS-1, we have joined the two ranges defined in (2-5) arbitrarily by a smooth curve.* The range $10\log\Omega_2' \gtrsim -45$ for HF-3 in Fig. 2-6 corresponds to the range where we have supposed an acoustic field predominates, and therefore we disregard this segment

*The abscissas at which the two curves of (2-5) would intersect is indicated by marks in Fig. 2-6. The coefficient η has been taken constant and equal to 0.71.

with regard to comparing with the curves for the FS-1. We see that the HF-3 and FS-1 curves, have, in fact, been brought nearer coalescence than in the plot of $10\log\pi_o'$ vs $10\log\omega_o$ of Fig. 2-2. Also, we note that the curves for the FS-1 at different speeds coalesce fairly well with one another except in a range $10\log\Omega_2' \lesssim -46$ where $\omega\delta_*/U_\infty$ may be too small for form (2-2) to apply. This latter range for the FS-1 may thus be discarded also with reference to the comparison with the HF-3 curves.

We thus suggest that a major reason for discrepancy among the curves for (1) HF-3 and USL 43, (2) Foxwell's elements, and (3) FS-1 in the range $3 < 10\log\Omega_o \lesssim 12$ in Fig. 2-2 is the increasing dependence of spectra on $\omega\nu/v_*^2$ as R_o decreases at fixed $\omega R_o/U_\infty$*,**.

---

*If the roughness of the surface in which any of these elements is situated is sufficiently great, as noted in the Appendix, we should expect that $\omega h/v_*$, in place of $\omega\nu/v_*^2$, is the pertinent variable. In this case the spectrum on the (Ω_o, π_o') plot would not be lowered as much relative to a larger element as if the surface were smooth. Here h denotes characteristic roughness height.

**If this discrepancy is thereby rectified, an apparent discrepancy will necessarily arise between the Franz element at the 10.5% point and HF-3, USL 43 in Fig. 2-2.

3. G and D Elements

Reliable noise autospectra are now available for Elements G5, G7, and G9 of Sea Chest 2 at 0, 10, 20 and 30 kt (Figs. 3-1 to 3). The general character of the results for the recessed element G5 remain as described previously, keynoted by the rise in noise above 2 khz at 20 kt and disappearance of this hump at 30 kt. This hump at 20 kt appears, but to a much subdued extent, for the flush element G7, and degenerates to a mere leveling tendency for the higher, hull-mounted flush element G9.*

In the low-frequency range up to 2 khz, over which the speed and frequency dependency of the G elements remains fairly regular, for 20 and 30 kt the recessed element G5 is quieter than G7 by 6 to 11 db. Toward the lower part of this interval (~0.2 khz), G7 in turn at 20 and 30 kt is a few db quieter than G9, but nearly the same further on in frequency. G9 in this frequency interval measures noise nearly equal to that on an element, e.g. LF-1, in the lower-positioned LF array; at 30 kt in the same frequency interval G9 measures noise several db lower than LF-1.

The striking speed-dependent hump at high frequency in the noise on G5 has been tentatively attributed to that due to bubble flow in the neighborhood of Sea Chest 2 (Refs. 5,4). In Figs. 3-4 to 7 are shown the apparent lower boundaries of the bubble-infested area along the hull, as obtained from photographic data, for head and following sea runs at 15, 20, 25, and 30 kt. The bubble area at 15 and 20 kt appears just to envelope Sea Chest 2 down to its lower boundary. At 25 and 30 kt, on the other hand, roughly the upper half of the sea chest is typically enveloped. The trace of the boundary line across the sea chest is inclined somewhat below the horizontal in the rearward sense.

We may expect that bubble noise, in contrast to noise due to the turbulent boundary layer (TBL), will depend substantially on heading, maneuver, and sea state and be subject also to considerable

* In the high-frequency range Figs. 3-1 to 3 show considerable variations of noise on G5, G7, and G9 even at zero speed.

statistical (time) variation. Fig. 3-8 shows two noise spectra (Runs 347A and 347B) for G5 at 20 kt computed from data taken on different days at different sea states (0 and 1).* In the range 2 to 5 khz these spectra differ by as much as 8 db while coinciding well at lower frequency. The corresponding results for element G8 are shown in Fig. 3-9, and a similar difference is seen to occur.

Noise spectra for G5 at 15 and 25 kt are compared in Fig. 3-10 for different headings. Above 2 khz, for 25 kt there is a striking difference ranging to 10 db. No appreciable difference occurs at 15 kt, on the other hand. The curve for 25 kt at 90° nearly coincides above 2 khz with the 15 kt curves. It is suggested that in the two runs at 15 kt and the 90° run at 25 kt the sea chest surface at G5 was enveloped by a bubble stream of maximum density, whereas in the 0° run at 25 kt, this element escaped the maximum effect. A similar comparison for element G8 is shown in Fig. 3-11. The differences at both 15 and 25 kt in this case are moderate.

We note from the geometry of the element configuration that whenever elements G5 and G6 lie within the bubble-infested region, so also do G7 and G8 and also G9 and G10. In order to account for the apparent increasing progression of high-frequency bubble noise at 20 kt from element G9 to G7 to G5, we might suppose that the intensity of bubble noise is not uniform over the infested area, but has a maximum near the lower boundary.*

Regarding the possibility that bubbles contribute significantly to noise on the layer-covered D elements at Sea Chest 1, Fig. 3-4 indicates that at 15 kt the lower boundary of the bubble-infested area may pass close to the upper edge of Sea Chest 1, especially at its aft portion. At higher speeds the bubble boundary passes well above this sea chest.

* We disregard the spectra for runs 340A and 340B shown in Fig. 3-8 as corresponding to questionable gain settings.

Fig. 3-12 compares the noise on element D1 at 15 and 25 kt for different headings. For 15 kt the spectrum for heading 90° lies well above that for 0° over the entire frequency range, the difference reaching a maximum of 15 db at 2.3 kHz. For 25 kt, on the other hand, there is very little difference between 0° and 90°. A similar comparison is made for element D2 in Fig. 3-13. In this case, at 15 kt the spectra are similar at low frequency and comparable above 6 khz, but at intermediate frequencies the spectrum for 90° lies above that for 0° by as much as 16 db at 2 kHz. As in the case of D1, for 25 kt there is little difference between 0° and 90°. Furthermore, the levels at 15 kt for 90° on both D1 and D2 are comparable with the levels at 25 kt. In view of the relative distance of the bubble boundary at 15 and 25 kt, it is suggested that for 15 kt the 90° heading results in close proximity of bubbles and hence high noise relative to 0°, but that for 25 kt the effect of heading on relative bubble proximity and hence noise is minimal.

If we attribute the variations in question to bubble noise, we observe that this noise in the case of the D elements is apparently spread over a broad frequency range, but in ths case of the G elements largely confined to frequencies above 1.5 khz. This result would imply a broader distribution of bubble sizes, in particular more relatively large bubbles, in the neighborhood of Sea Chest 1 than in that of Sea Chest 2.

Addendum

An investigation by analog data-processing methods has been made of the time variation of the noise levels in various frequency bands for elements G-5 and LF-9. Results are shown in Figs. 3-14 to 3-17 for speeds 10 and 15 kt. These may be broadly summarized as follows.

In frequency bands up to 2 khz the rms deviation for LF-9 is only ~1 db at 10 kt and ~2 db at 15 kt. In these bands for G-5 the rms deviation is ~2 db at 10 kt and ~3 db at 15 kt. In frequency bands from 2 khz to 13 khz the rms deviation for LF-9 at 10 kt is likewise only ~1 db. At 15 kt, however, the deviation for LF-9 is irregular and large, perhaps ~5 db. Furthermore, the variations in level in the several frequency bands distinguished above 2 khz the correlations of levels among bands is poor, e.g. where the level between 2 and 5 khz is extraordinarily high the level between 5 and 13 khz is often extraordinarily low. In the case of G-5, even at 10 kt there is great variation in level for the high-frequency bands, especially from 3.2 to 13 khz, deviations being ~5 db. These deviations, however, are well correlated among frequency bands and furthermore display a distinct periodic effect with frequency 0.3 to 0.5 hz. At 15 kts, for G-5 the variations remain great, rather greater for 2 to 5 khz than for 5 to 13 khz, but the periodic structure is less pronounced and shifted to ~0.6 hz. likewise, unlike LF-9, the levels are well correlated among frequency bands.

The larger time variation of noise level for G-5, especially at high frequency, accords with the supposition of a large bubble-noise contribution and the broad peak in the high-frequency region. It is noteworthy that the increase of noise with frequency at 15 kt (for the band divisions used) persists through times of low as well as high total noise.

The comparison between G5 and LF-9 with regard to the degree of correlation of variations in different high-frequency bands seems to say that, in the case of the recessed element G5, when a large number of bubbles of one size are located so as to produce much noise on G5, so also are a large number of bubbles of other sizes, but in the case of LF-9 a large number of bubbles of one size are often

located so as to produce much noise while those of another size are not and conversely; yet the extent of variations and the periodicity for both elements are comparable.

Listening to the noise records in question likewise gives the impression of some non-uniform high-frequency noise in the case of G-5 at 10 and 15 kt and some especially tinkly noise in the case of LF-9 at 15 kt. LF-9, we observe, is the highest element of the LF array and probably, of this array, the element nearest the bubble-infested region.

The severe variations in spectral level in the case of G-5 do not inspire confidence in the significance of the instances in Figs. 3-8 to 3-13 where several spectra nearly coincide.

4. Summary

In summary and conclusion, we state:

1. The noise on the 5"-diameter HF and LF flush elements at the higher speeds ($\gtrsim$ 15 kt) is dominated by the direct TBL contribution roughly up to the frequency where the negative slope decreases; this frequency typically is $\sim 0.8(U_\infty/20\text{ kt})$ khz. In the corresponding domain of the dimensionless variable $\omega R_o/U_\infty$, the scaling law for these large elements conforms fairly well to the form $P(\omega/2\pi)/\rho^2 v_*^4 U_\infty^{-1} R_o = f(\omega R_o/U_\infty)$; hence, in this domain the TBL noise is not expected to decrease with distance aft and, for moderate changes in R_o, may vary roughly as R_o^{-3}.

2. In this same domain of $\omega R_o/U_\infty$, the noise spectra for much smaller elements does not scale in the manner stated above, but are lower than that scaling law would predict on account of the influence of the parameter $\omega\nu/v_*^2$.

3. In the frequency domain above the decrease in spectral slope for the 5" elements, the noise is thought not to be due primarily

* These conclusions supersede those of Ref. 4 where in conflict.

to the direct TBL pressure but to some other speed-dependent noise field. For a given ship configuration the noise still depends on $\omega R_o/U_\infty$ somewhat in accord with the aforementioned scaling law, but changes with ship configuration, e.g. Purvis to Albacore.

4. The noise referred to in 3 is tentatively attributed mainly to noise radiated by flow-induced hull vibrations. This attribution, however, appears to conflict somewhat with the measured cross-spectral magnitudes and perhaps with the low noise on the recessed element G5 at 30 kt. It is a central necessity to fathom the problems of this domain.

5. The noise measured by large elements in the vicinity of sea chests 1 and 2, especially the latter, for certain speeds and frequency ranges is highly variable, and bubble noise is considered to be the cause. The variations with heading and run at different speeds appear to have a plausible correlation with indicated bubble flow paths. In the case of sea chest 2 the variable noise is largely confined to the frequency range above 1.3 khz.

6. At speeds and frequencies and for time cuts where bubble noise apparently does not dominate the spectrum on element G5, for speeds $\geq$ 20 kt, the noise on this recessed element is lower than that on similar flush elements by ~10 db. The recessed position of the element is tentatively concluded to reduce TBL noise relative to flush mounting in a substantial frequency range of interest by such an amount.*

5. Recommendations for Further Processing and Analysis

We give in summary preliminary general recommendations for PURVIS II with reference to tasks to be performed in the second cut and also some which can be pursued, if not completed, in the present first cut.

* The consequent effect on signal-to-noise ratio depends on the result of a reliable in situ calibration, and on the spatial correlation of the interior field, in a configuration of actual interest.

5.1 Noise Data Processing and Analysis

1. Process and analyze for more elements, with the widest available distribution in position, in order to establish better the dependence on circumferential position and other coordinates related to proximity to the surface and to bubble-flow paths.

2. Process and analyze more data with a view to reliably distinguishing systematic from statistical variations and, where the latter are concerned, making full use of the data, with the aid of the computer generate averaged results with minimum standard deviations. This point refers mainly to elements where variations between spectra computed for different time cuts are indicated to be minimal.

3. In the case of elements whose spectra are known to be seriously time dependent, presumably on account of bubble effects, process auto- and cross-spectra with explicit regard to whether the spectral level during a given time cut is high or low. This course will permit a consistent and discriminating analysis. In particular, correlate variations in cross-spectra with variations in auto-spectra.

4. Make more extensive comparison of PURVIS II results with the wide variety of ship and laboratory noise data available, including those of PURVIS I, with particular reference to the perplexing high-frequency range. Employ the types of dimensionless plot that correspond to TBL pressure scaling laws that may have validity in various domains. Main objectives here are the correct identification of dominant noise sources in various domains and prediction of the dependence of TBL noise spectra on distance aft, hydrophone size, and, with reference to covered elements, properties of the dome or layer. Study auto- and cross-spectra further for possible resolution of uncertainties associated with the frequency range above the slope-decrease point in the spectra on 5" elements. Estimate speed-dependent acoustic noise on these elements.

5. By use of analog data-processing techniques, produce time histories of noise level in selected frequency bands for further elements and conditions. Also, listen to the recorded noise for evidence of bubbles, etc.

6. Study the variation with heading and other conditions, of the lower boundary of the hull area covered by bubbles, as obtained from photographic data, and attempt to correlate with noise measurements.

7. By use of analog data, cross-correlate measured noise in a given frequency band with bow-probe or other ship-motion output. (Cut 2 only)

8. Write digital program for beam-forming and analyze apparent angular distributions of noise measured by HF and LF arrays under various conditions in selected frequency band. (Cut 2 only)

5.2 Transmission Data Processing

In the first cut of PURVIS II no appreciable processing and analysis of transmission runs have been performed. In these runs signals transmitted from strut-mounted transducers were received by the ship-mounted hydrophones, the amplitudes and phases of these received signals being affected by whatever bubbles were present in the region between transmitting and receiving elements.

We propose a plan for processing in the second cut that is based on use of analog data processing. At a later stage, when some results are available, however, it may appear worthwhile to construct programs for further digital processing. It is suggested to produce the following types of output from the analog data.

1. Visual records of envelope of received signals.
2. Amplitude distribution of envelope
3. Cross-correlation between envelopes received at two elements.
4. Cross-correlation of clipped signal with clipped signal for same element at zero speed .
5. Cross-correlation of signal envelope with bow-probe or other ship-motion output.
6. Cross-correlation of signal envelope with noise level on same element in a frequency band excluding that of the transmitted signal.

Items 1 and 2 will provide information concerning frequency, duration, and extent of signal dropout for a given element at given speed, heading, and maneuver. Item 3 will indicate the degree and spatial scale of correlation between such dropouts at different elements for optimum time delay. Item 4 will provide information on signal phase shift due to transmission through bubbles similar to that on signal amplitude provided by item 1; if the phase shift is smaller than that due to relative strut motion, however, only an upper limit on phase shift will be obtained. Item 5 will test the extent of the mentioned correlation associated with the dependence of bubble production and paths on ship motion and illuminate the latter relation. Item 6, together with 5, will provide further indication of instances where noise measured in a given band is due to bubbles.

APPENDIX A

REMARKS ON THE SCALING OF TURBULENT BOUNDARY-LAYER PRESSURE FLUCTUATIONS

Most generally, the spectrum of average pressure on a circular area of radius R_o in a plane bounding an incompressible turbulent flow must have the form

$$(A\text{-}1) \qquad P(\omega/2\pi) = \rho^2 R_o U_\infty^3 F(\omega R_o/U_\infty, R_o/\delta_*, \omega\nu/v_*^2).$$

In the limit of vanishing area, i.e., $\omega R_o/U_\infty \to 0$, $R_o/\delta_* \to 0$, this must reduce to

$$(A\text{-}2) \qquad P(\omega/2\pi) \to P_o(\omega/2\pi) = \rho^2 \delta_* U_\infty^3 G(\omega\delta_*/U_\infty, \omega\nu/v_*^2).$$

Well known considerations have been adduced (e.g., see Ref. 1) to indicate that in some high-frequency regime characterized by $\omega\nu/v_*^2$, the latter form probably becomes more simply

$$(A\text{-}3) \qquad P_o(\omega/2\pi) = \rho^2 \nu v_*^2 H_+(\omega\nu/v_*^2),$$

independent of δ_*. Likewise, in some opposite, low-frequency regime characterized by $\omega\delta_*/U_\infty$, the form becomes rather

$$(A\text{-}4) \qquad P_o(\omega/2\pi) = \rho^2 \delta_* U_\infty^3 H_-(\omega\delta_*/U_\infty),$$

independent of ν/v_*. More recently, it has been suggested that P_o, in a broad regime, may indeed be independent of both lengths δ_* and ν/v_* and therefore have the form

$$(A\text{-}5) \qquad P_o(\omega/2\pi) \propto \rho^2 v_*^4 \omega^{-1},$$

which is the particular form constituting the intersection of forms (A-3) and (A-4) where we regard v_*/U_∞ as a constant and

neglect its weak dependence on Reynolds number*.

By related arguments (e.g., see Ref. 1), it is indicated that, for a large area such that $\omega R_o/U_\infty \gg \pi$ at not too small $\omega\nu/v_*^2$, the high-wavenumber (convective) contribution to $P(\omega/2\pi)$ has the form

$$(A\text{-}6) \qquad P_+(\omega/2\pi) = (\omega R_o/U_\infty)^{-3}\rho^2\nu v_*^2 L_+(\omega\nu/v_*^2),$$

independent of δ_*. Further, the function $L_+(x)$ may be approximately identified, to within a factor of the order of unity, with $H_+(x)$ in (A-3). The remaining, low-wavenumber contribution to $P(\omega/2\pi)$ for such an area, at least when $R_o \gtrsim \delta_*$, may rather have the form

$$(A\text{-}7) \qquad P_-(\omega/2\pi) = \rho^2\delta_* U_\infty^3 M(R_o/\delta_*, \omega\delta_*/U_\infty),$$

independent of ν/v_*. If, at the same time, R_o is not much larger than δ_*, the latter form may become roughly

$$(A\text{-}8) \qquad P_-(\omega/2\pi) = (\omega R_o/U_\infty)^{-2}\rho^2\delta_* U_\infty^3 N(\omega\delta_*/U_\infty);$$

if, on the contrary, $R_o \gg \delta_*$ (still for an incompressible fluid), we expect instead

$$(A\text{-}9) \qquad P_-(\omega/2\pi) = (\omega R_o/U_\infty)^{-3}\rho^2\delta_* U_\infty^3 S(\omega\delta_*/U_\infty).$$

Recently it has been suggested (Ref. 3) that, even for an area of arbitrary size, in a broad range of frequency the total spectrum $P(\omega/2\pi)$ $(= P_- + P_+)$ is actually nearly independent of both δ_* and ν/v_*, having therefore, by (A-1), the form

$$(A\text{-}10) \qquad P(\omega/2\pi) = \rho^2 R_o v_*^3 f(\omega R_o/U_\infty),$$

---

*Since (5) is thus a special case of (3) and of (4), it is futile to attempt to deny these latter to affirm the former. A similar remark applies to (A-6) and (A-10) (cf. Ref. 3).

where, in the present account, we again do not distinguish between v_* and U_∞ apart from a factor regarded as constant. The sum of (A-6) and (A-8) or (A-9) itself reduces to form (A-10) provided $L_+(x) \propto x^{-1}$ and $N(x) \propto x^{-1}$ or $S(x) \propto x^{-1}$; in such case in (A-10) we would have

$$f(x) = a_+ x^{-4} + a_- x^{-3} \text{ if (A-8) holds, or}$$
$$f(x) = (a_+ + a_-) x^{-4} \text{ if (A-9) holds,} \qquad \text{(A-11)}$$

where a_+ and a_- are constants. In the former case, $P(\omega/2\pi)$ would contain terms respectively proportional to $R_o^{-3} U_\infty^7 \omega^{-4}$ and $R_o^{-2} U_\infty^6 \omega^{-3}$, and in the latter, the entire $P(\omega/2\pi)$ would be proportional to $R_o^{-3} U_\infty^7 \omega^{-4}$. It is possible, however, that (A-10) is valid more generally than (A-6) - (A-9) or that the reverse is true.

If $\omega R_o/c$ is not small relative to unity, where c is the speed of sound in the fluid, we must relax the condition of incompressibility. Likely forms can once again be proposed for $P(\omega/2\pi)$, but we refrain from such discussions here. It suffices to observe that the quantity $\omega R_o/c$ measures the importance of the compressibility effect,* but the actual threshold of importance of this effect must depend on a numerical coefficient whose value is presently accessible only to experiment.

The surface bounding the TBL has been implicitly assumed above to be smooth. Suppose instead the area surrounding the element is densely rough with characteristic roughness height h such that $h \gtrsim 6\nu/v_*$, i.e. height h rather greater than the depth of the viscous sublayer on a smooth surface. In this event we may expect that wherever ν occurred above, e.g. in Eq. (A-1), it should now be replaced by hv_*.

* Certain considerations indicate that, apart from $\omega R_o/c$, the quantity $(v_*/c)^2 (\omega R_o/U_\infty)^3$ may determine the relative magnitude of the compressibility effect.

REFERENCES

1. D. Chase, 23rd Navy Symposium on Underwater Acoustics, ONR Symp. Rept. ACR-115 (Conf.), p. 51; TRG tech. memo 011-TN-65-8 (unclass.), 1965.

2. P. Bradshaw, NPL Aero Rept. 1172, 1965.

3. J. H. Foxwell, A.U.W.E. Tech. Note 218/66, August, 1966

4. Purvis II Sea Trials Preliminary Data Analysis Report, TRG-023-TM-67-10, March, 1967 V. 2+3 = AD 044 689

5. Preliminary Analysis of Purvis I and II Acoustic Data, Hydrosystems, Inc., HI 67-21, April, 1967

6. D. Chase, unpublished

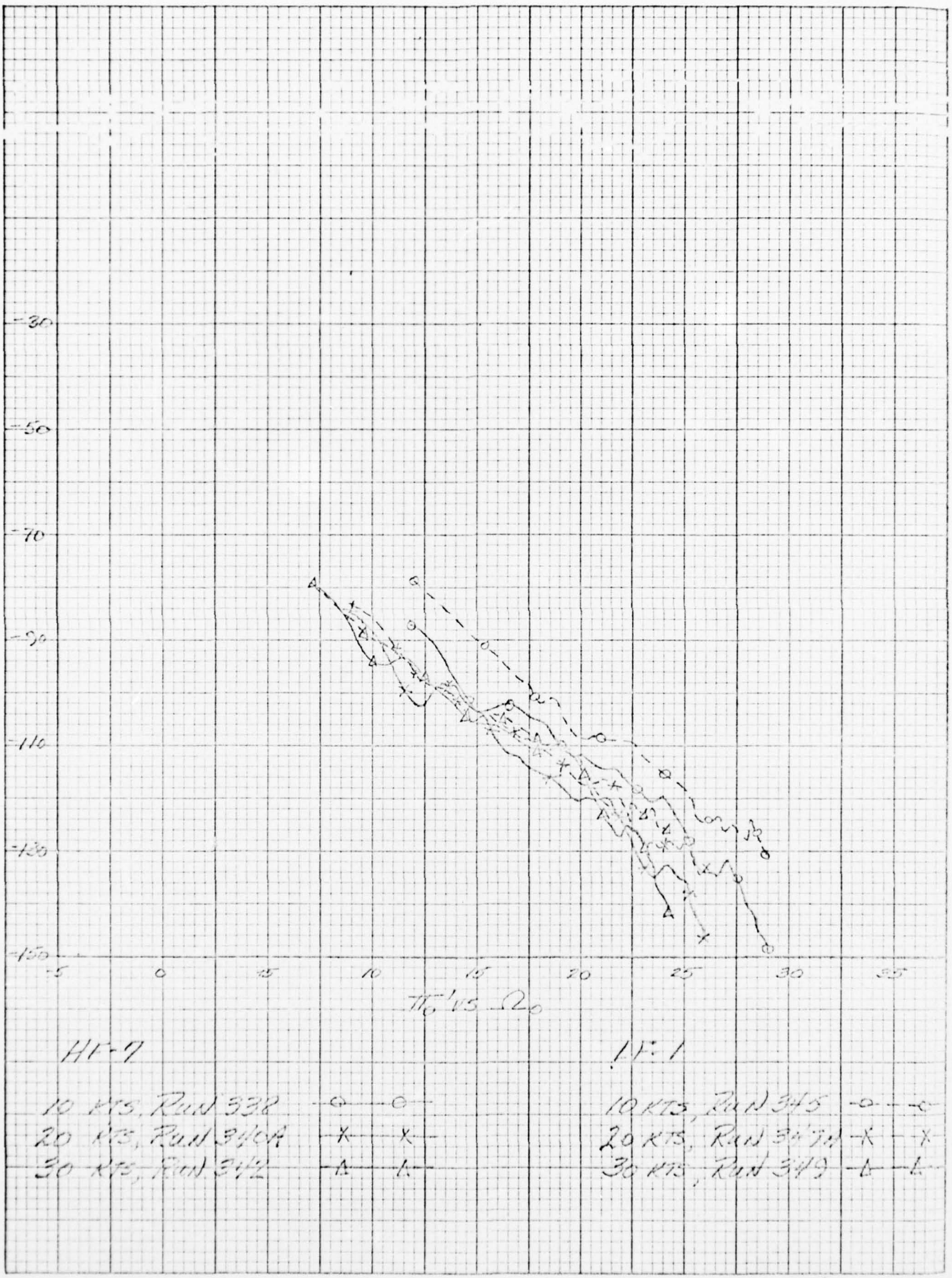

Fig. 2-1

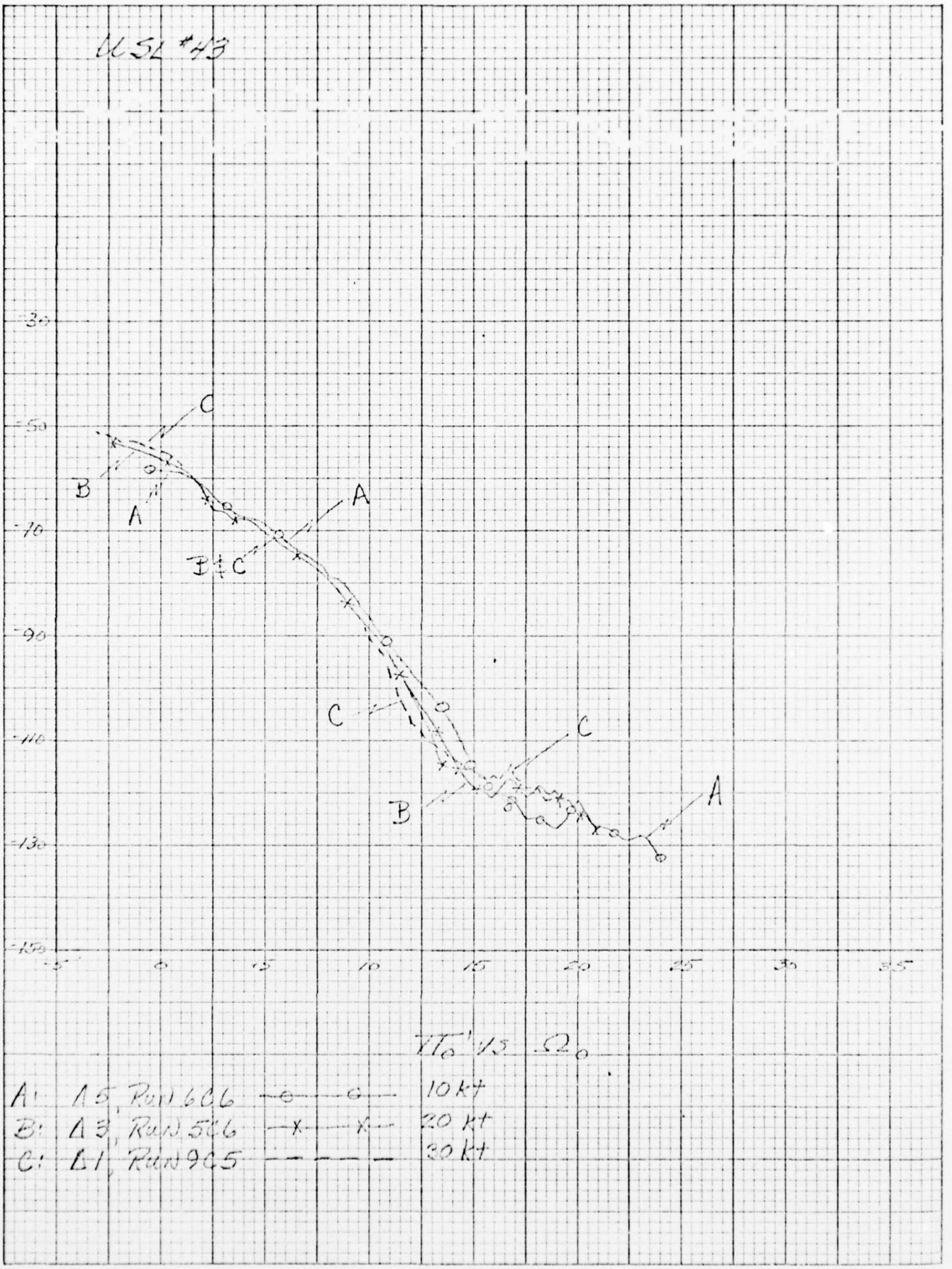
U 52 #43
-30
-50
-70
-90
-110
-130
-150
-5
0
5
10
15
20
25
30
35
A
B
C
A
B
C
C
B
A
V_o kts Ω_o
A: 15, Run 606 — 10 kt
B: 13, Run 586 — 20 kt
C: 11, Run 905 — 30 kt

Fig. 2-1A

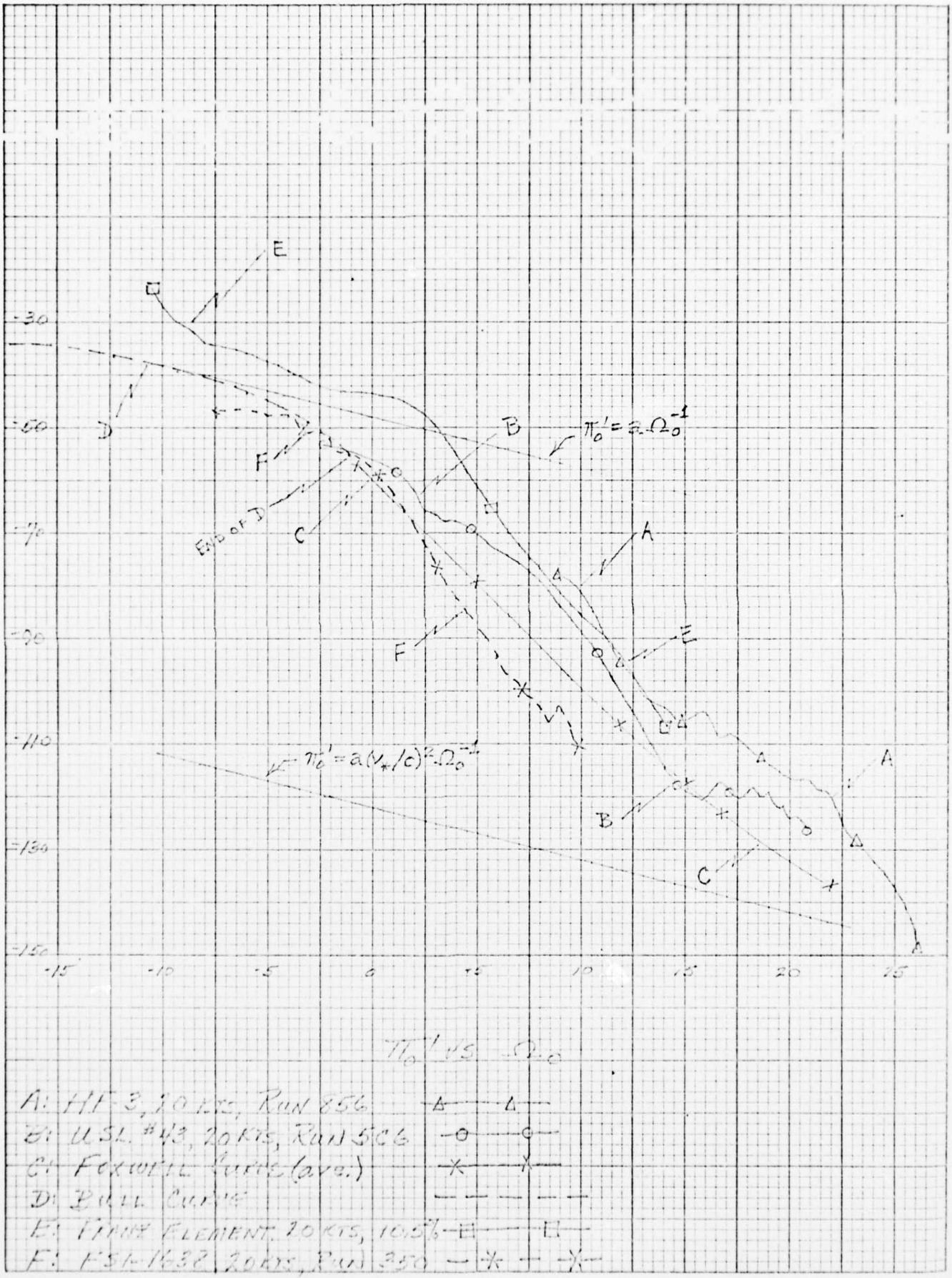

KEUFFEL & ESSER CO. 10 X 10 TO ½ INCH 46 1022 7½ X 10 INCHES MADE IN U.S.A.

FIG. 2-2

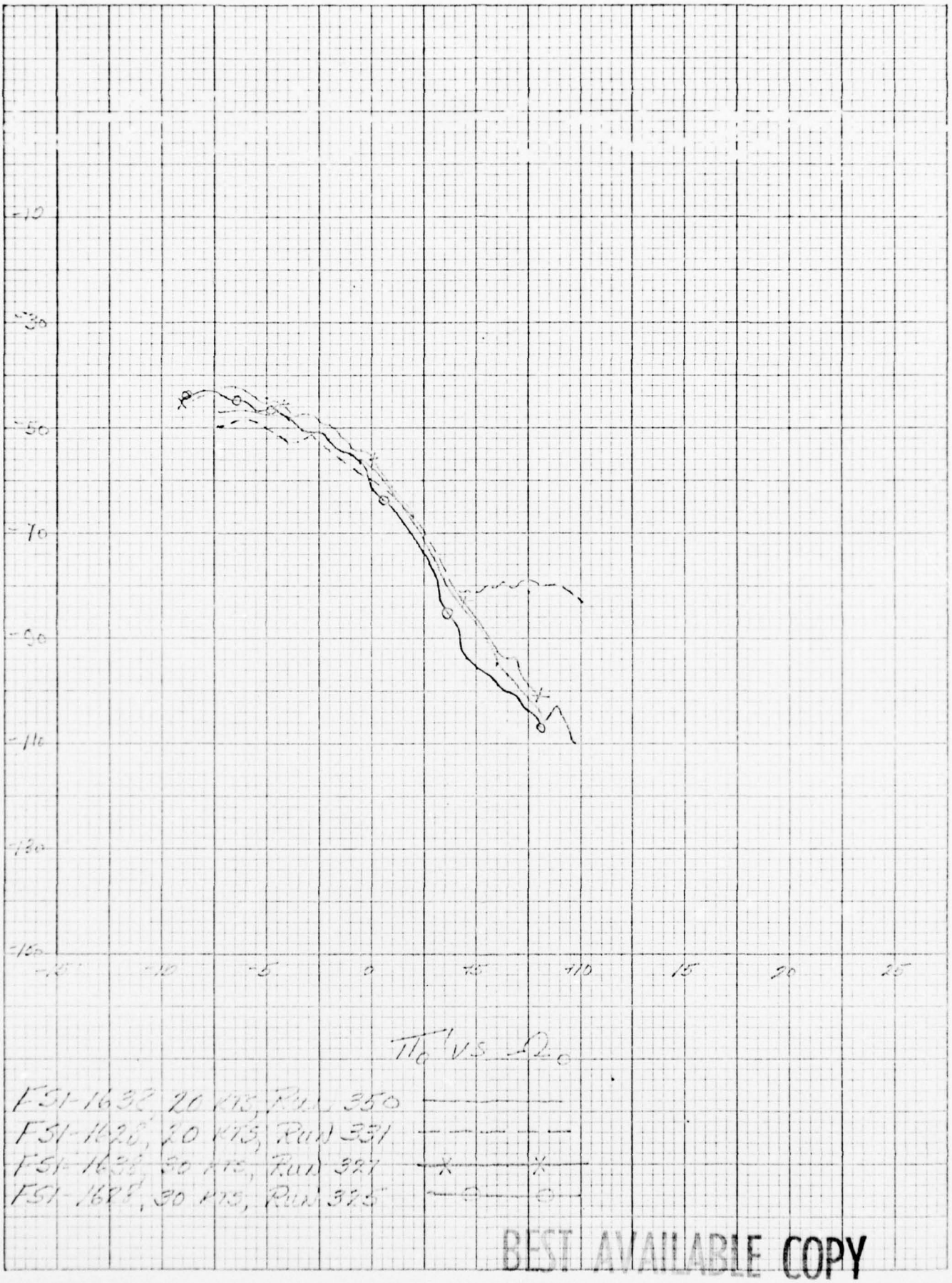

FIG. 2-3

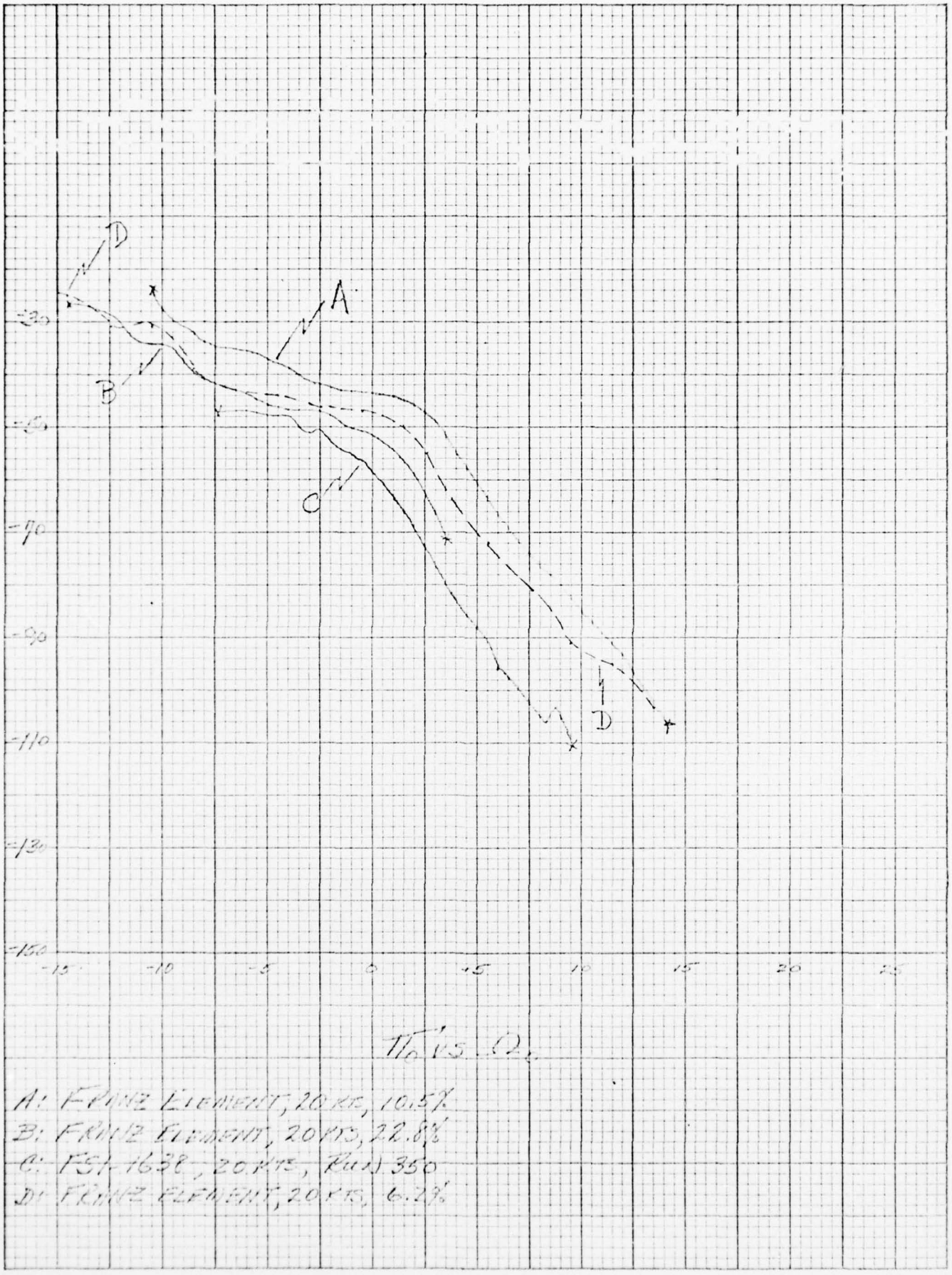

η_o vs. Q_1

A: Four Element, 20 KS, 10.5%
B: Four Element, 20 KS, 22.8%
C: FSF-1638, 20 KS, Run 350
D: Four-Element, 20 KS, 6.2%

Fig. 2-4

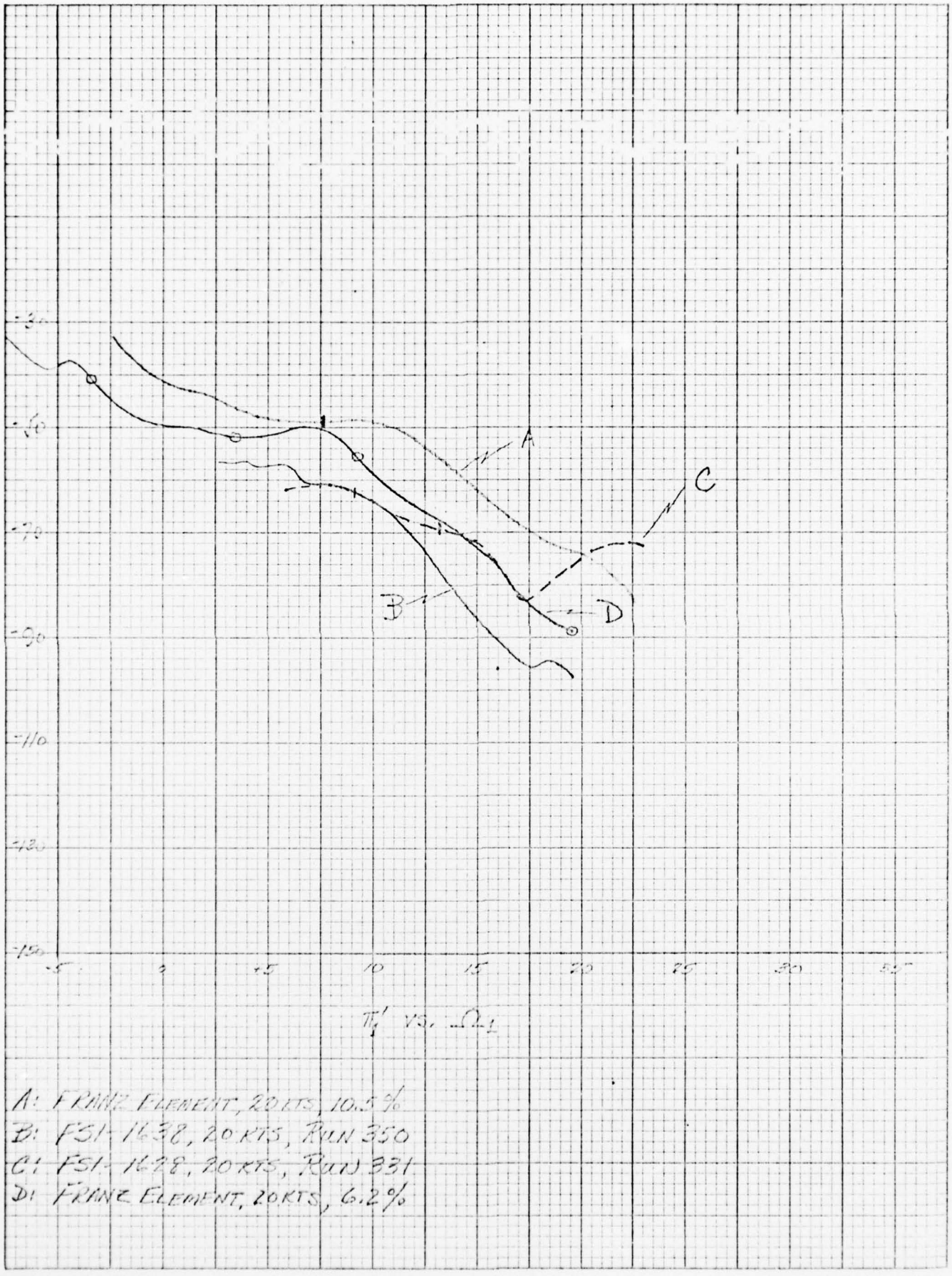

FIG. 2-5

FIG. 2-5A

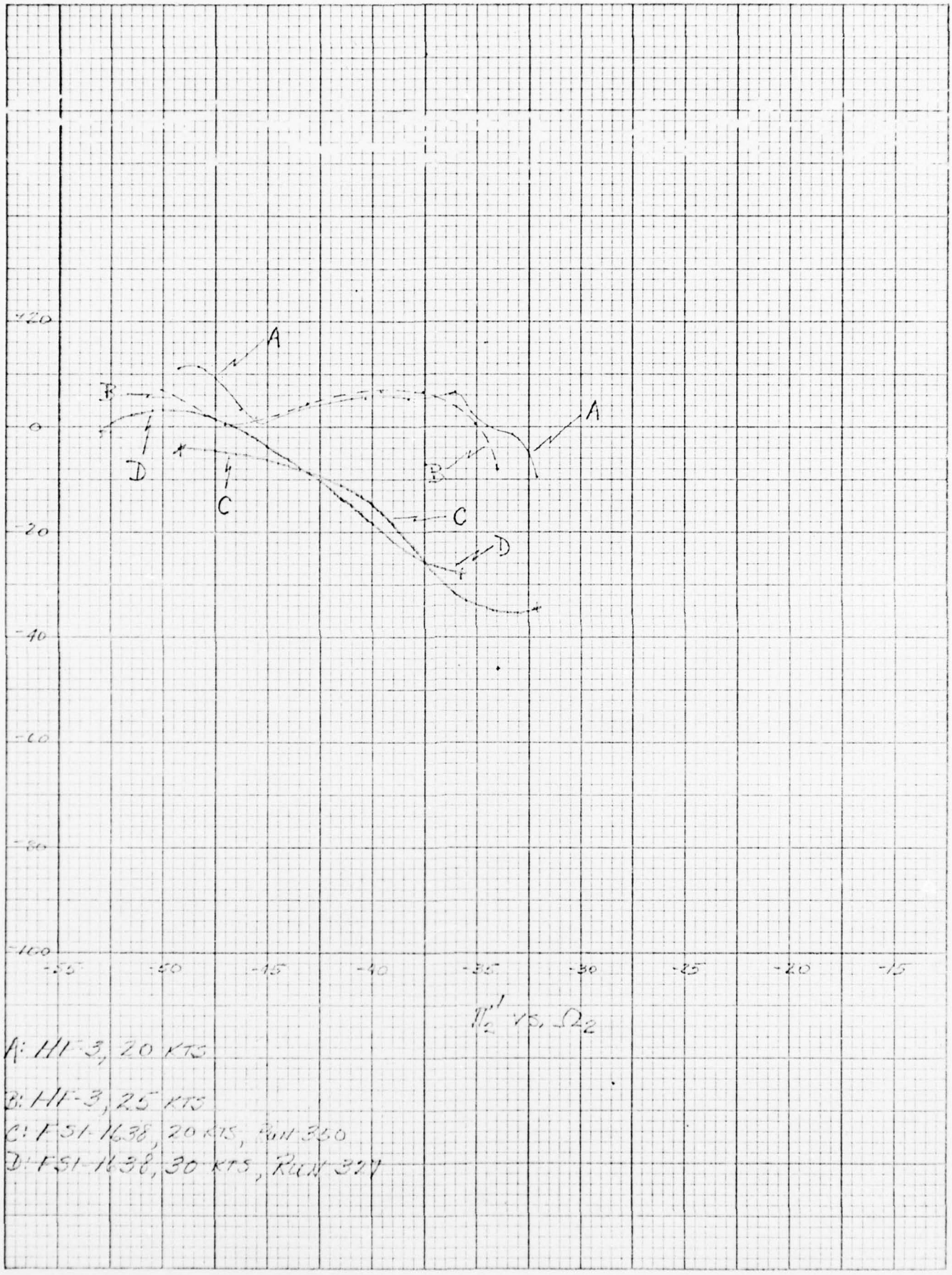

FIG. 2-6

4042

ELEMENT G-5

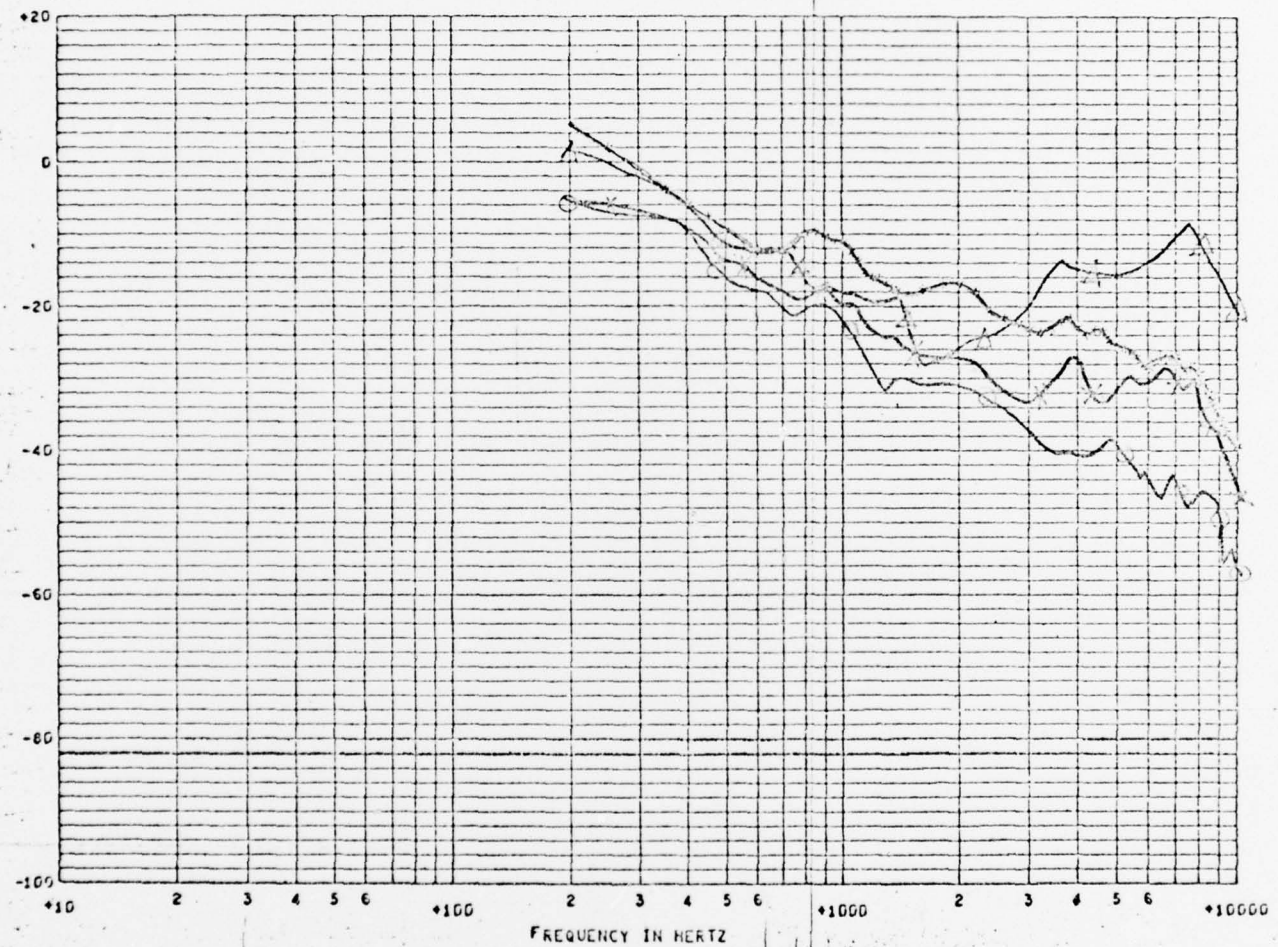

SPECTRUM DB REF 1 MICROBAR SQUARED TIMES SEC GXX LOW BAND CP209 - 63A HI BAND CP209 - 66A
RUN 349 START TIME 134500.0 SPEED 30 HEADING 000 W.R.T. SEA SEA STATE 1
TYPE SER NO COMMENTS
HYDRO G-5 SEA CH 2 093 11.25 00000

0 KTS, Run 348 — o — o —
10 KTS, Run 345 — x — x —
20 KTS, Run 347A — Δ — Δ —
30 KTS, Run 340 ——

Fig. 3-1

4362

ELEMENT: G-7

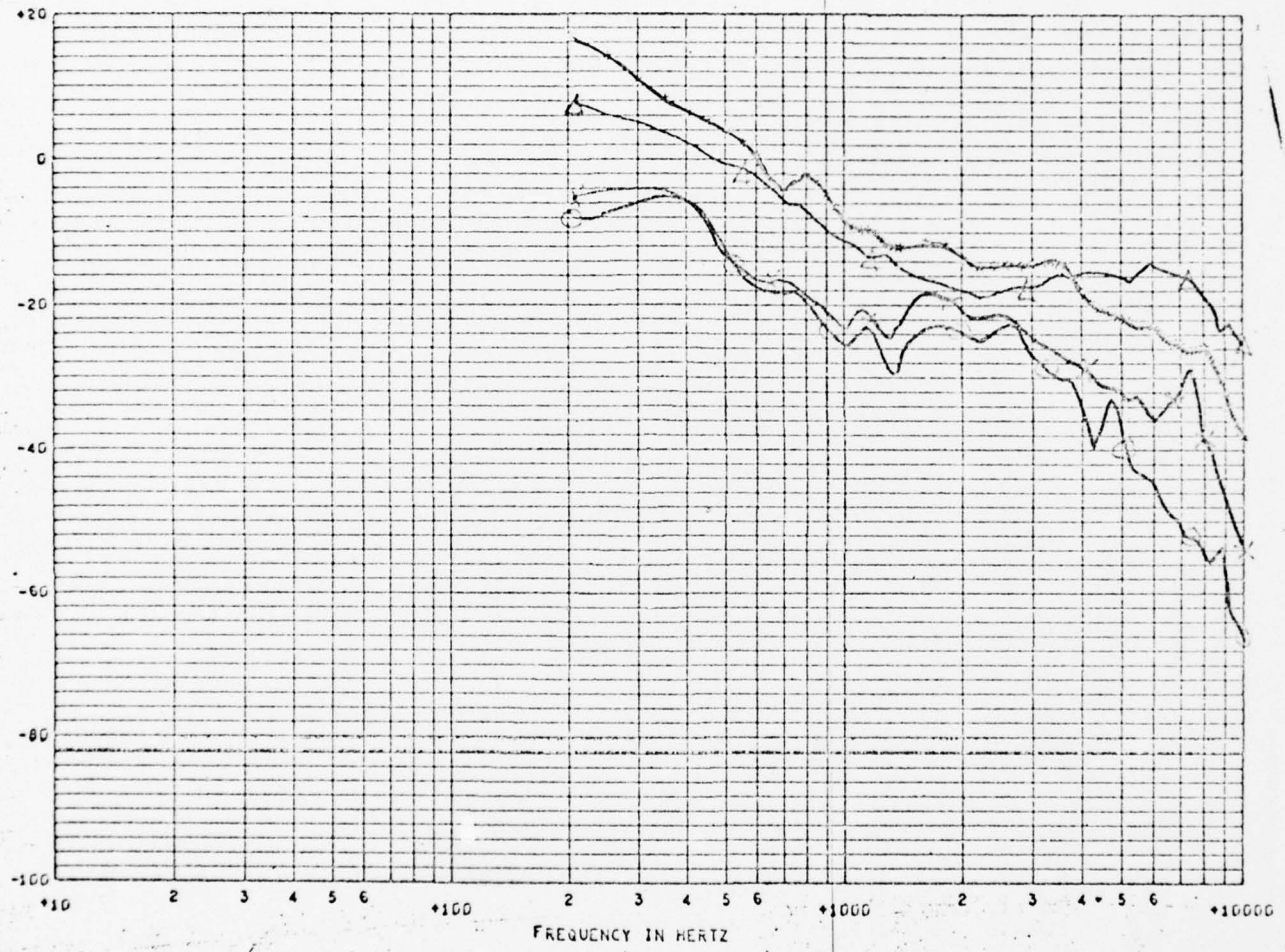

SPECTRUM DB REF 1 MICROBAR SQUARED TIMES SEC GXX LOW BAND CF209 - 64B HI BAND CF209 -. 67B
RUN 349 START TIME 13*56*00.0 SPEED 30 HEADING 000 W.R.T. SEA SEA STATE 1
TYPE SER NO COMMENTS
HYDRO G-7 SEA CH 2 098 11.75 00000

0 KTS, Run 343 —o—o—
10 KTS, Run 345 —x—x—
20 KTS, Run 347A —Δ—Δ—
30 KTS, Run 349 ———

Fig. 3-2

4062

ELEMENT: G-9

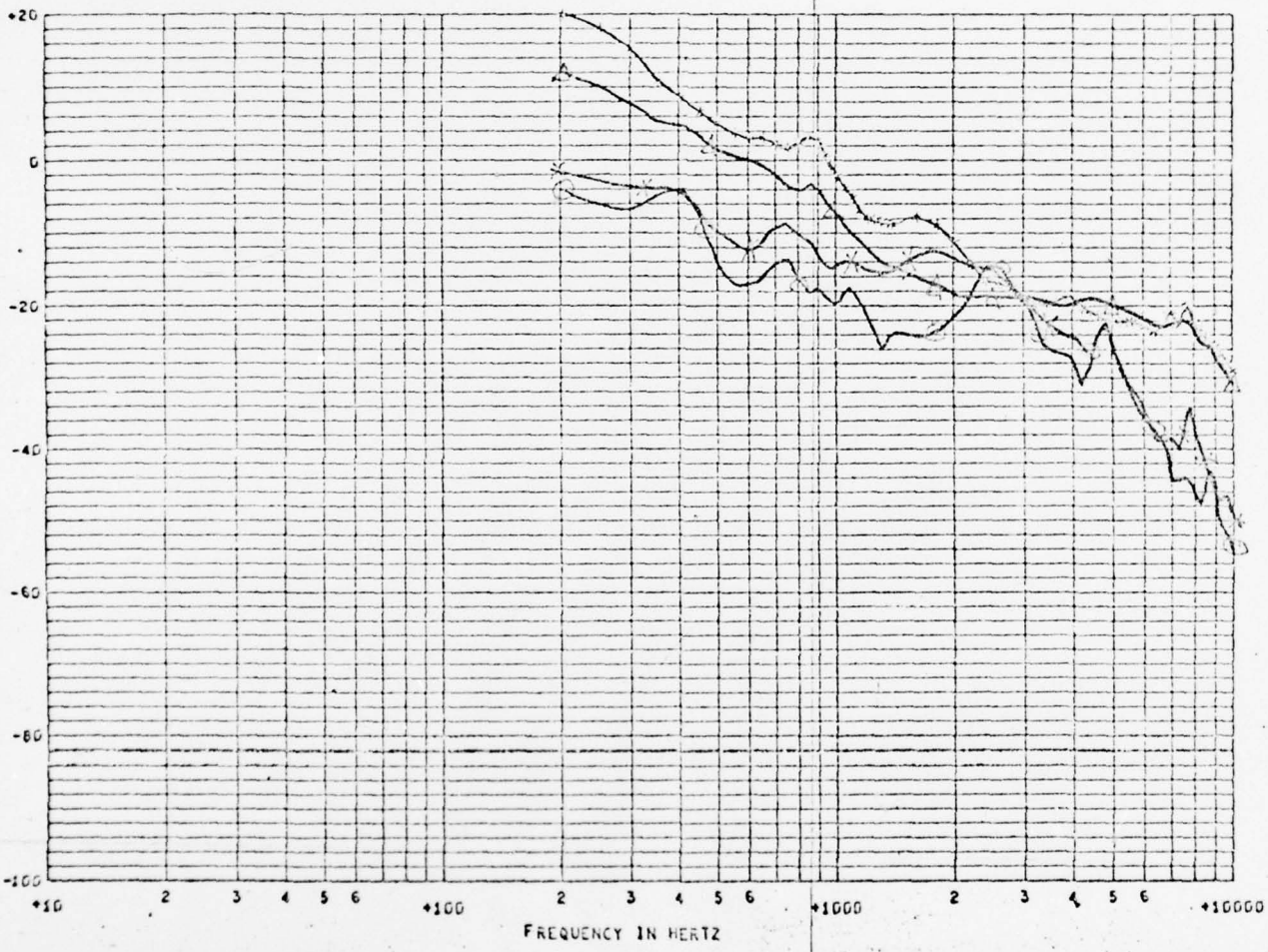

SPECTRUM DB REF 1 MICROBAR SQUARED TIMES SEC GXX LOW BAND CF209 - 70A HI BAND CF209 - 69A
RUN 349 START TIME 13*50*00.0 SPEED 30 HEADING 000 W.R.T. SEA SEA STATE 1

TYPE	SER NO	COMMENTS
HYDRO	G-9	SEA CH 2 D96 01.75

0 KTS, Run 343 —○—○—
10 KTS, Run 345 —×—×—
20 KTS, Run 347A —△—△—
30 KTS, Run 349 ———

Fig. 3-3

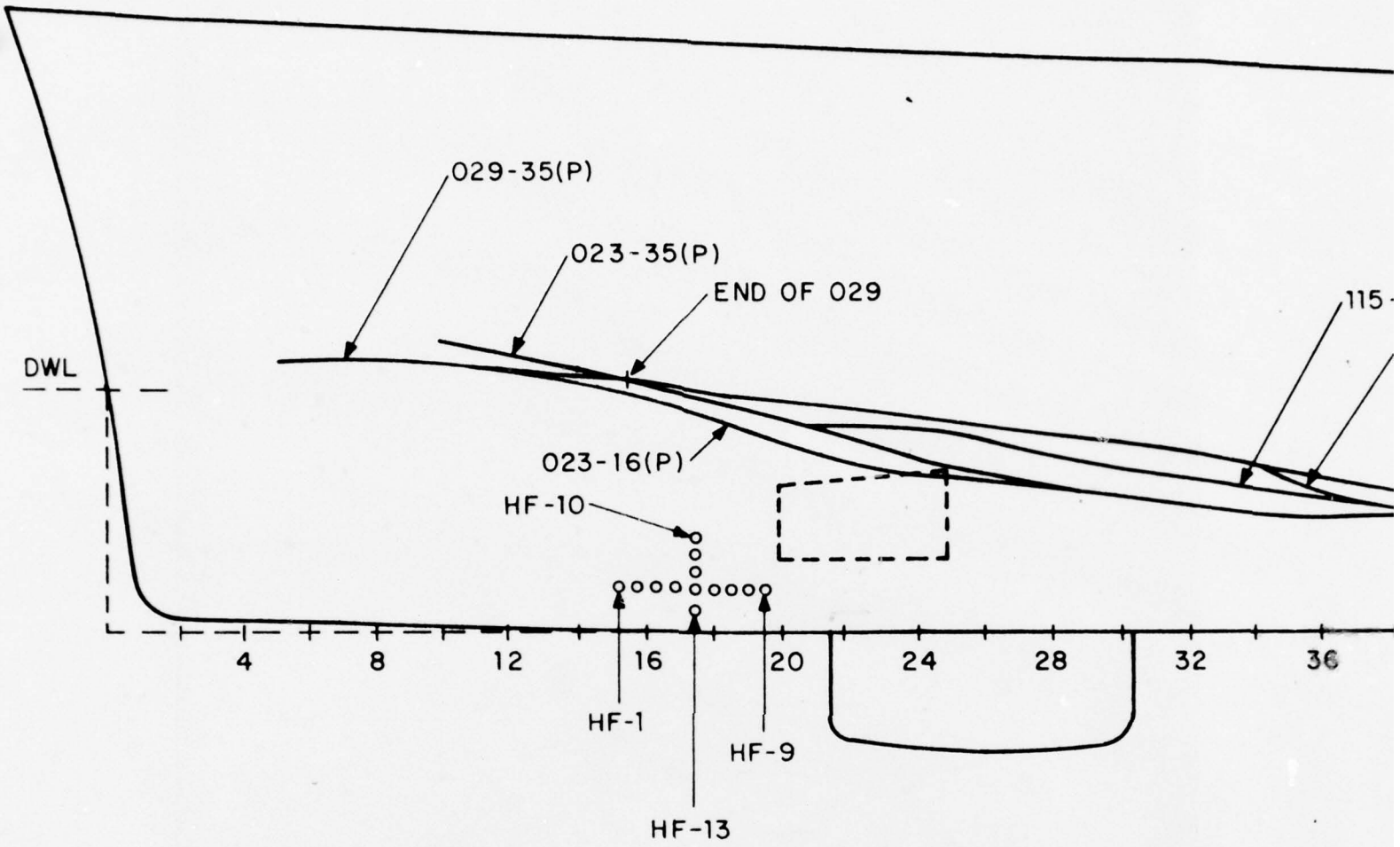

NOTE:

TRACES REPRESENT THE LOWEST EXTREMITY OF THE NATURAL SWEEPDOWN BUBBLE CLOUD FOR GIVEN RUNS (115, 217 ETC.) PHOTOGRAPHED BY 16 OR 35 MM CAMERAS.

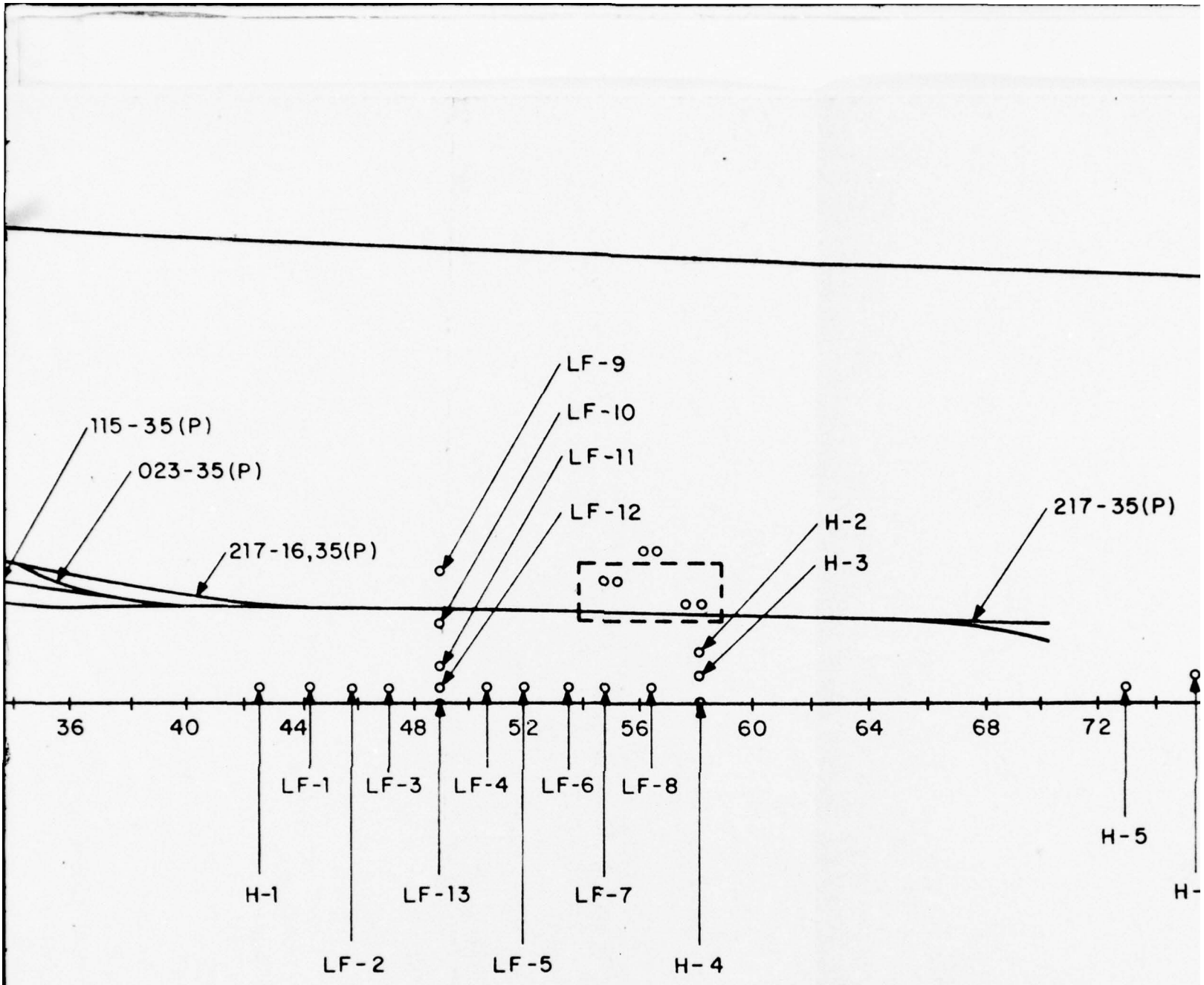
LF-9
LF-10
LF-11
LF-12
115-35(P)
023-35(P)
217-16,35(P)
H-2
H-3
217-35(P)
36
40
44
48
52
56
60
64
68
72
LF-1
LF-3
LF-4
LF-6
LF-8
H-5
H-1
LF-13
LF-7
H-
LF-2
LF-5
H-4

PURVIS II. 1

217-35(P)

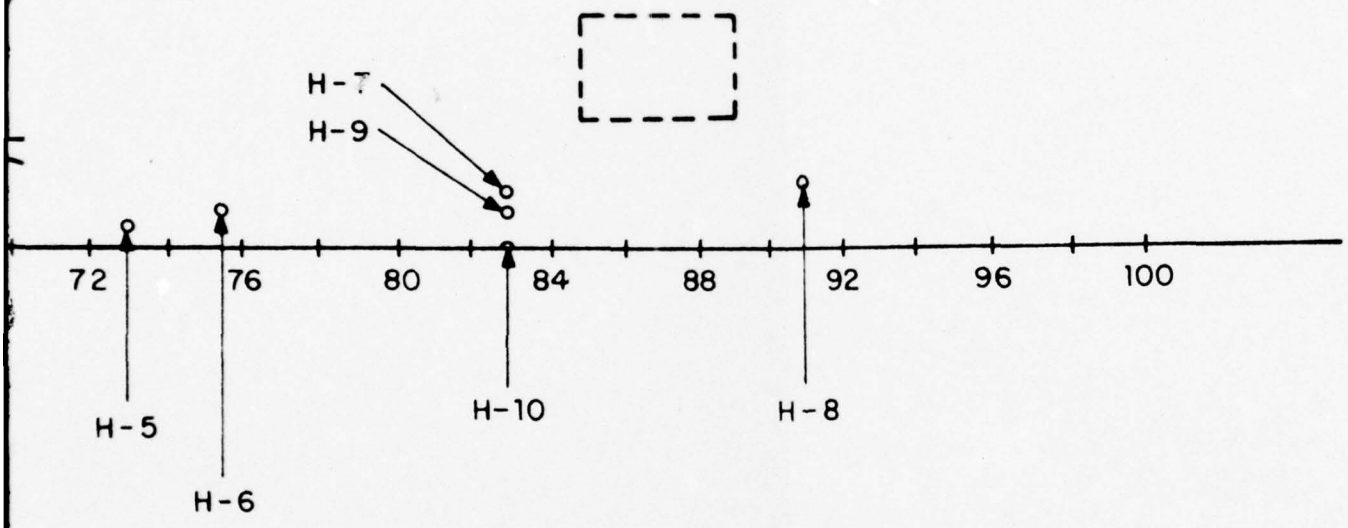

VIS II. 15 KNOTS - HEAD & FOLLOWING SEA RUNS ONLY

3

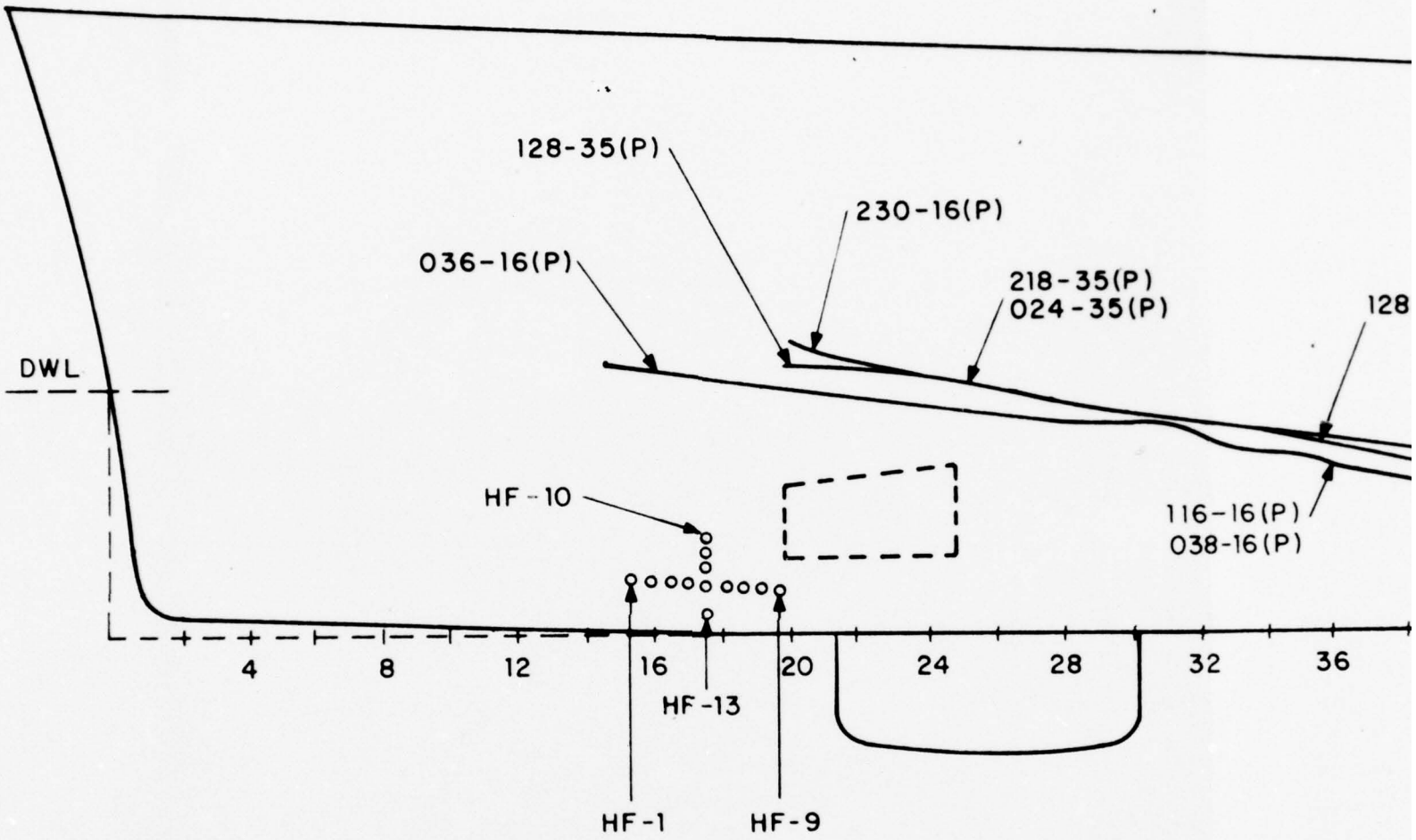

NOTE:

TRACES REPRESENT THE LOWEST EXTREMITY OF THE NATURAL SWEEPDOWN BUBBLE CLOUD FOR GIVEN RUNS (115, 217 ETC.) PHOTOGRAPHED BY 16 OR 35 MM CAMERAS.

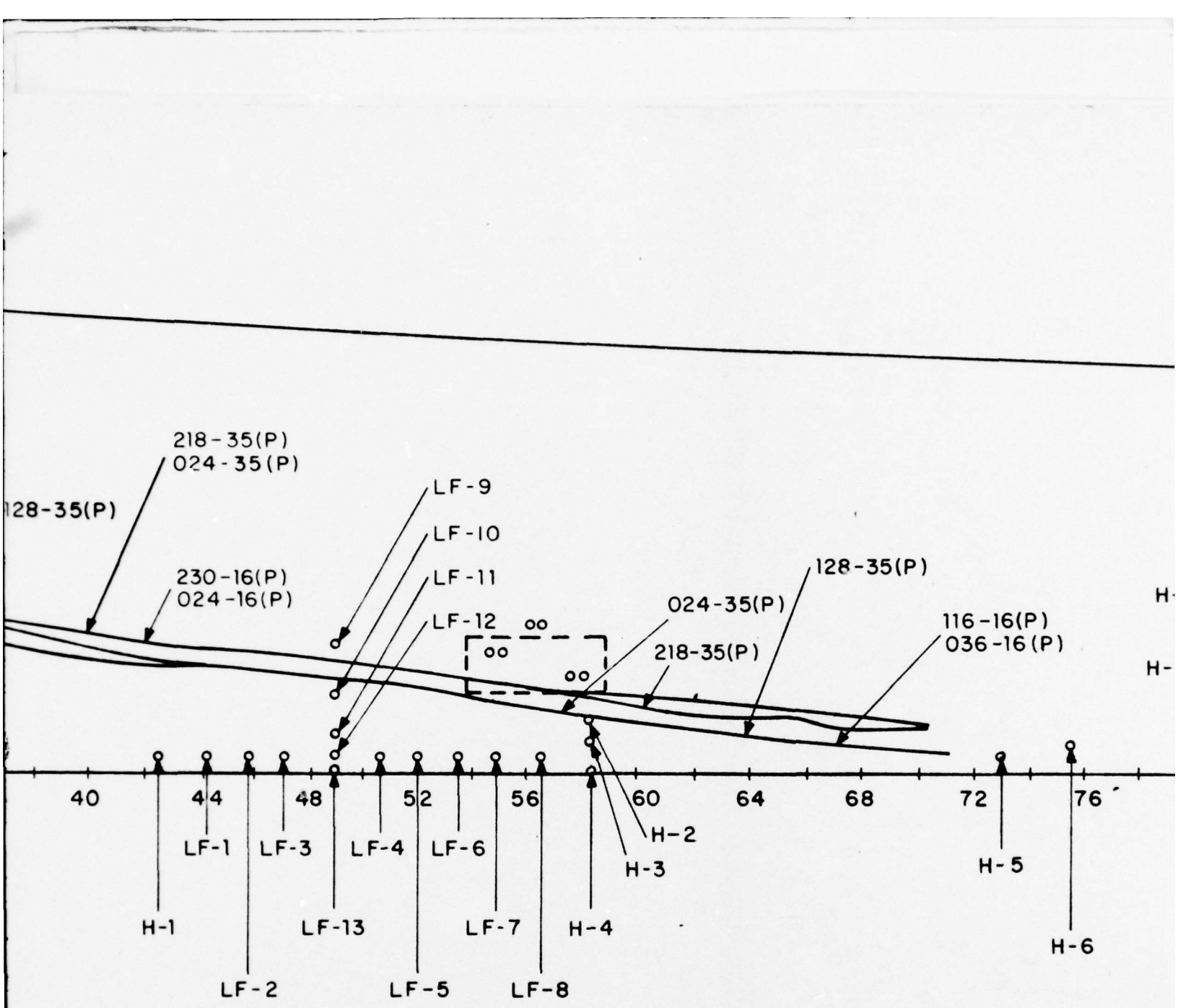

PURVIS II. 20 KNOTS

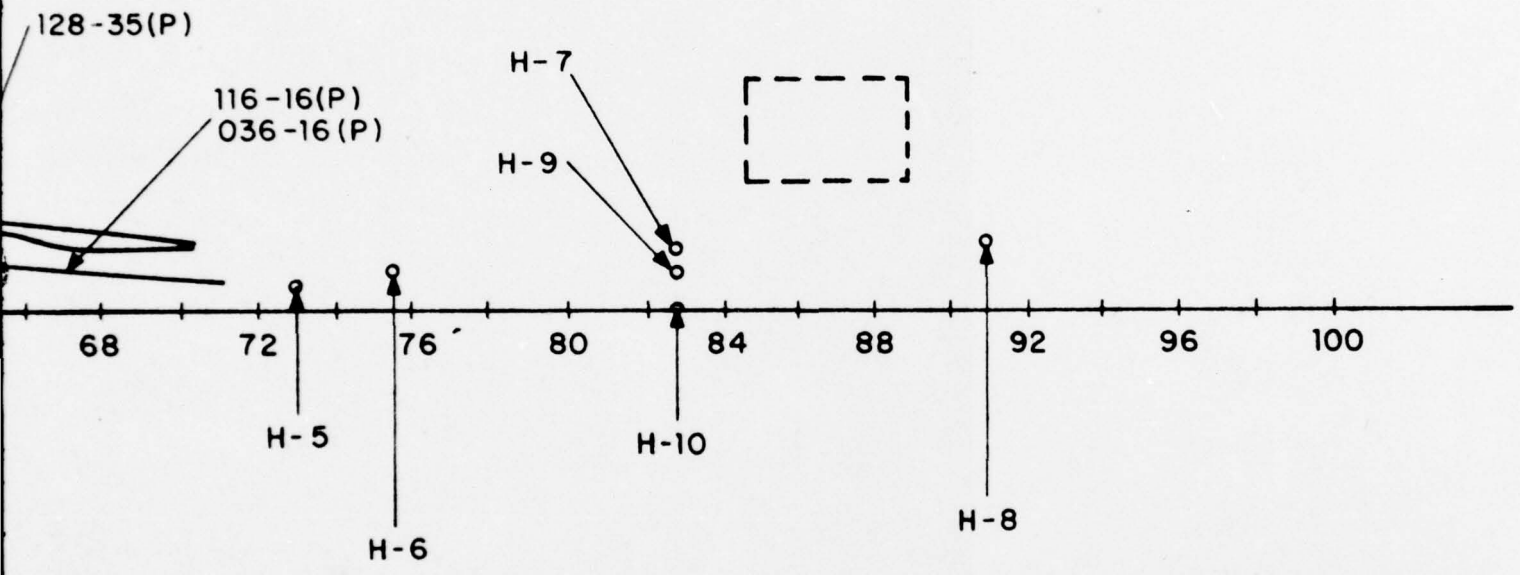

PURVIS II. 20 KNOTS-HEAD & FOLLOWING SEA RUNS ONLY

3

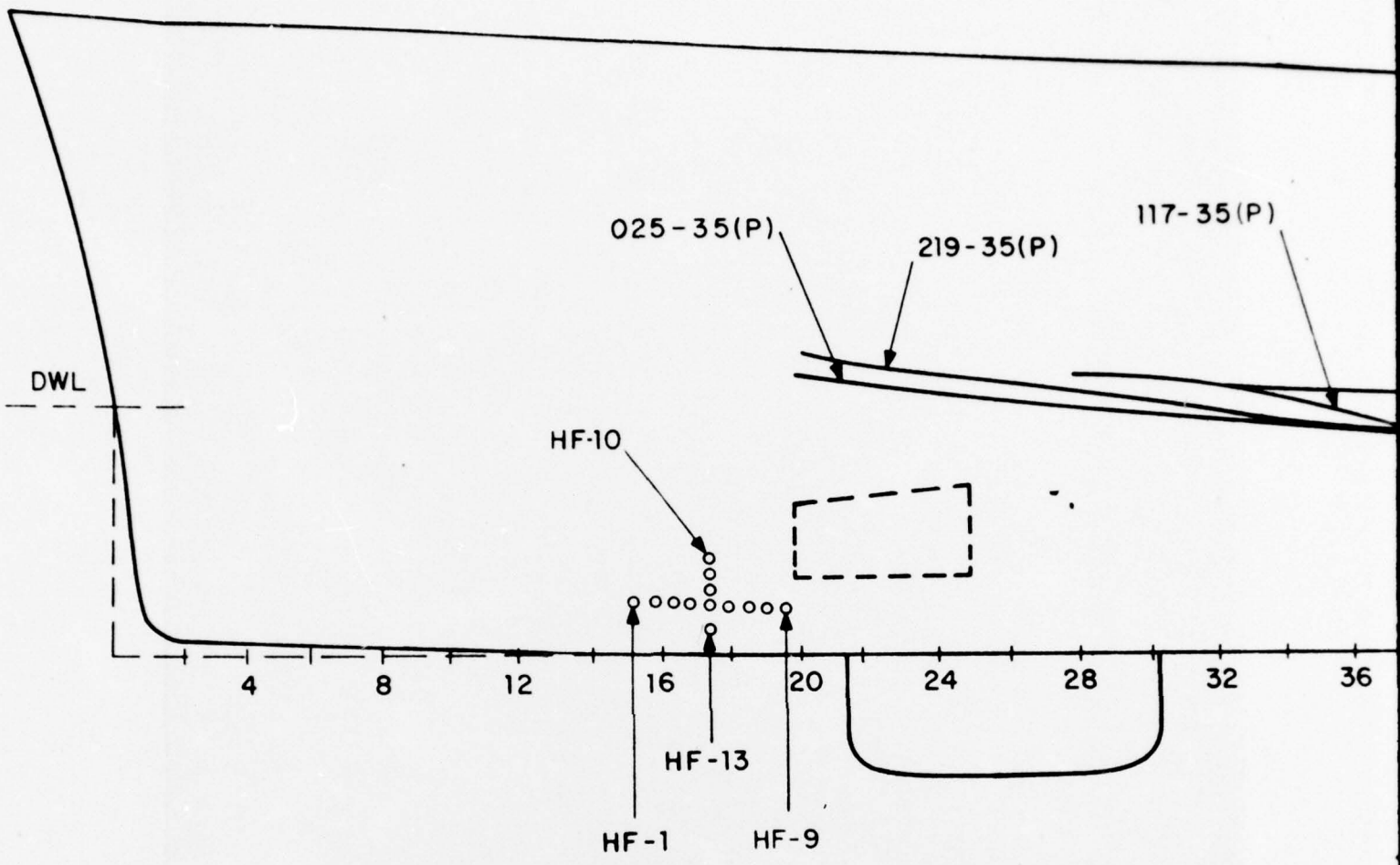

NOTE:
TRACES REPRESENT THE LOWEST EXTREMITY OF THE NATURAL SWEEPDOWN BUBBLE CLOUD FOR GIVEN RUNS (115, 217 ETC.) PHOTOGRAPHED BY 16 OR 35 MM CAMERAS.

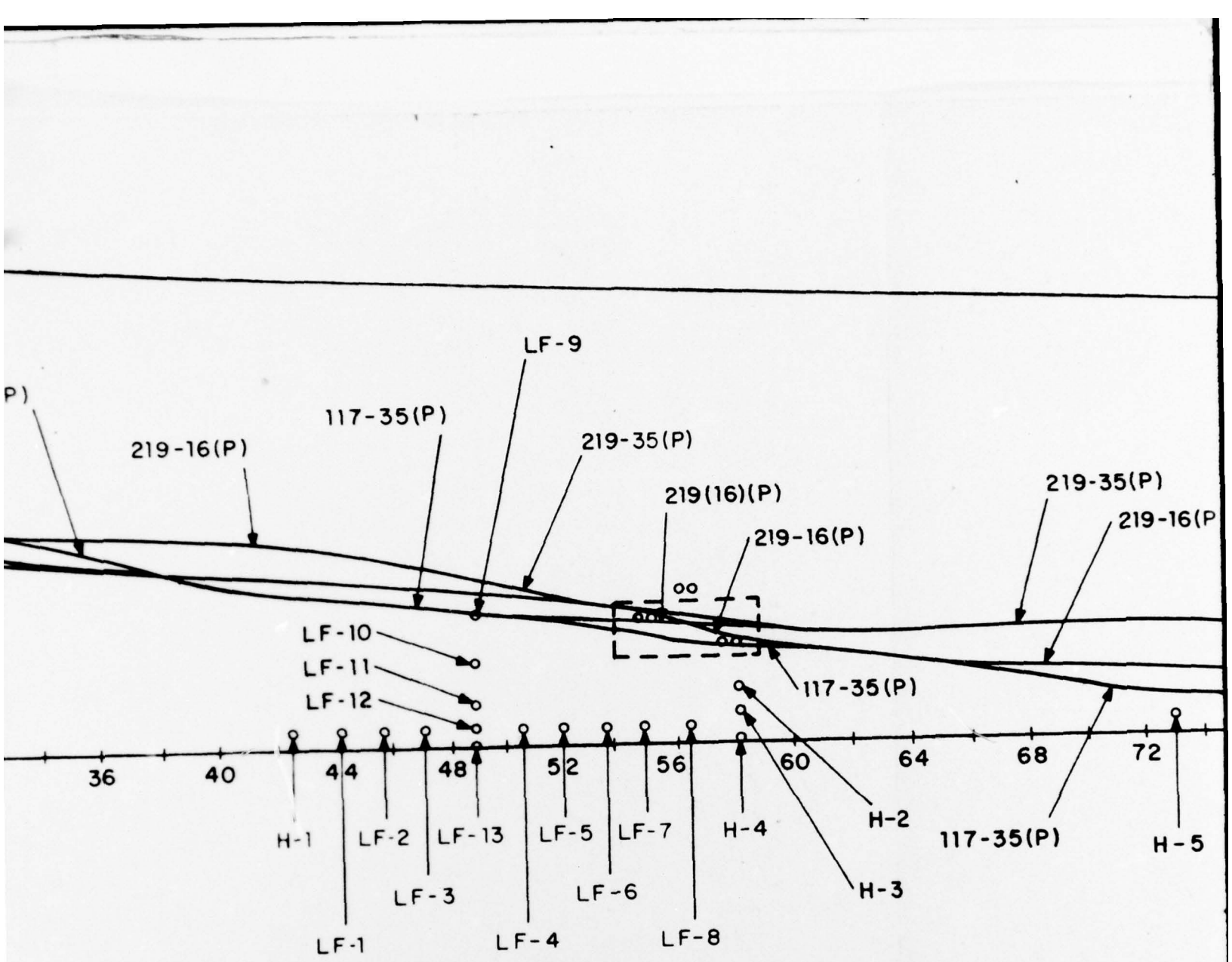
LF-9
P)
117-35(P)
219-16(P)
219-35(P)
219(16)(P)
219-16(P)
219-35(P)
219-16(P
LF-10
LF-11
LF-12
117-35(P)
36
40
44
48
52
56
60
64
68
72
H-1
LF-2
LF-13
LF-5
LF-7
H-4
H-2
117-35(P)
H-5
LF-3
LF-6
H-3
LF-1
LF-4
LF-8

PURVIS II.

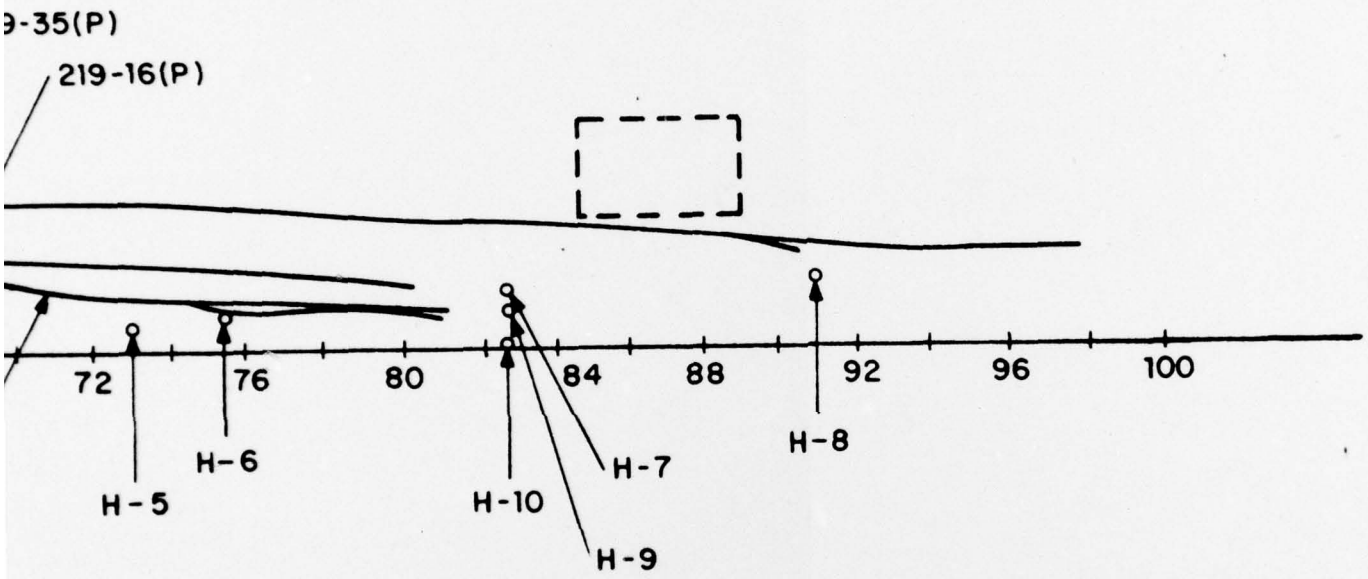

RVIS II. 25 KNOTS - HEAD & FOLLOWING SEA RUNS ONLY

3.

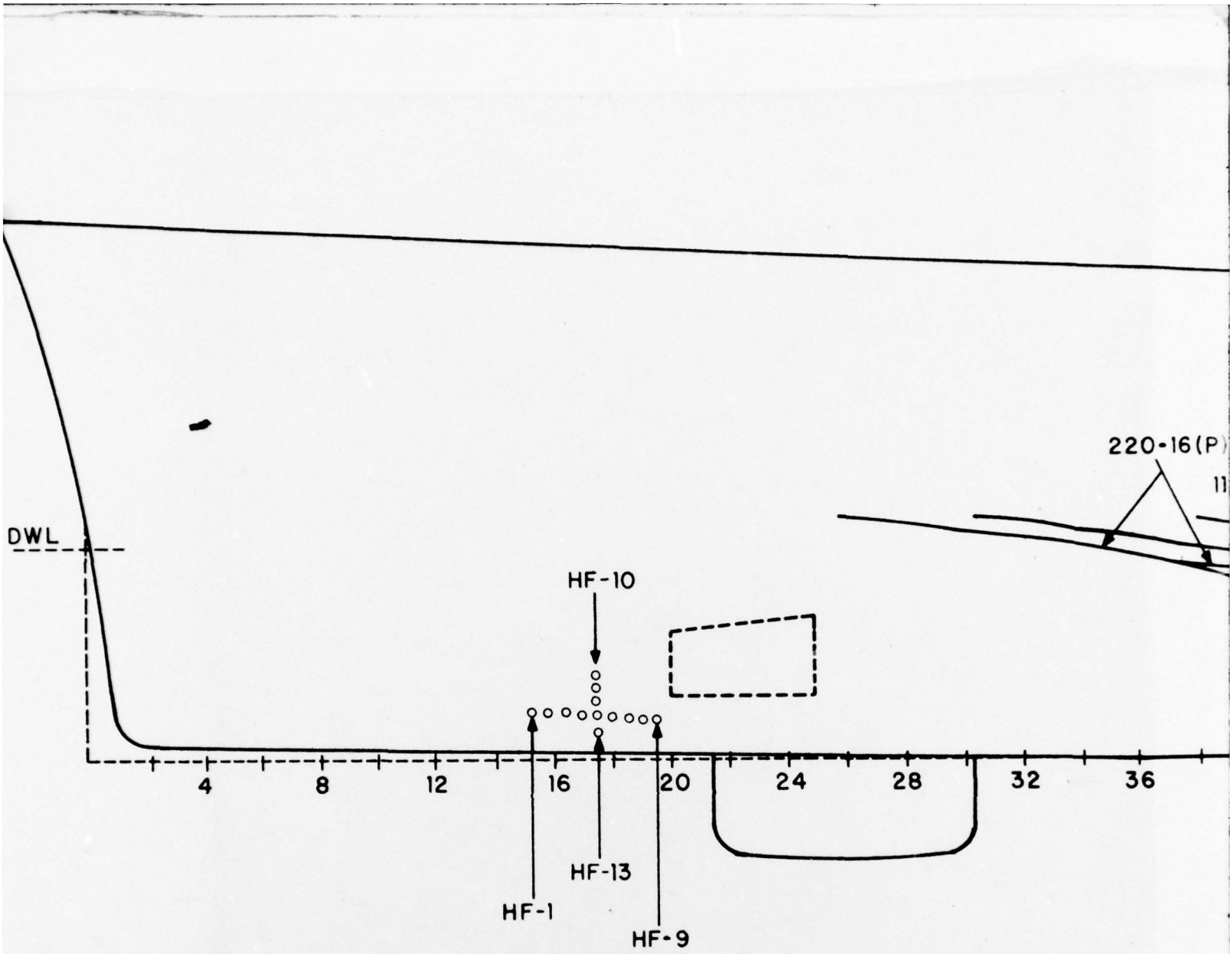

NOTE:
TRACES REPRESENT THE LOWEST EXTREMITY OF THE NATURAL SWEEPDOWN BUBBLE CLOUD FOR GIVEN RUNS (115,217 ETC.) PHOTOGRAPHED BY 16 OR 35 MM CAMERAS.

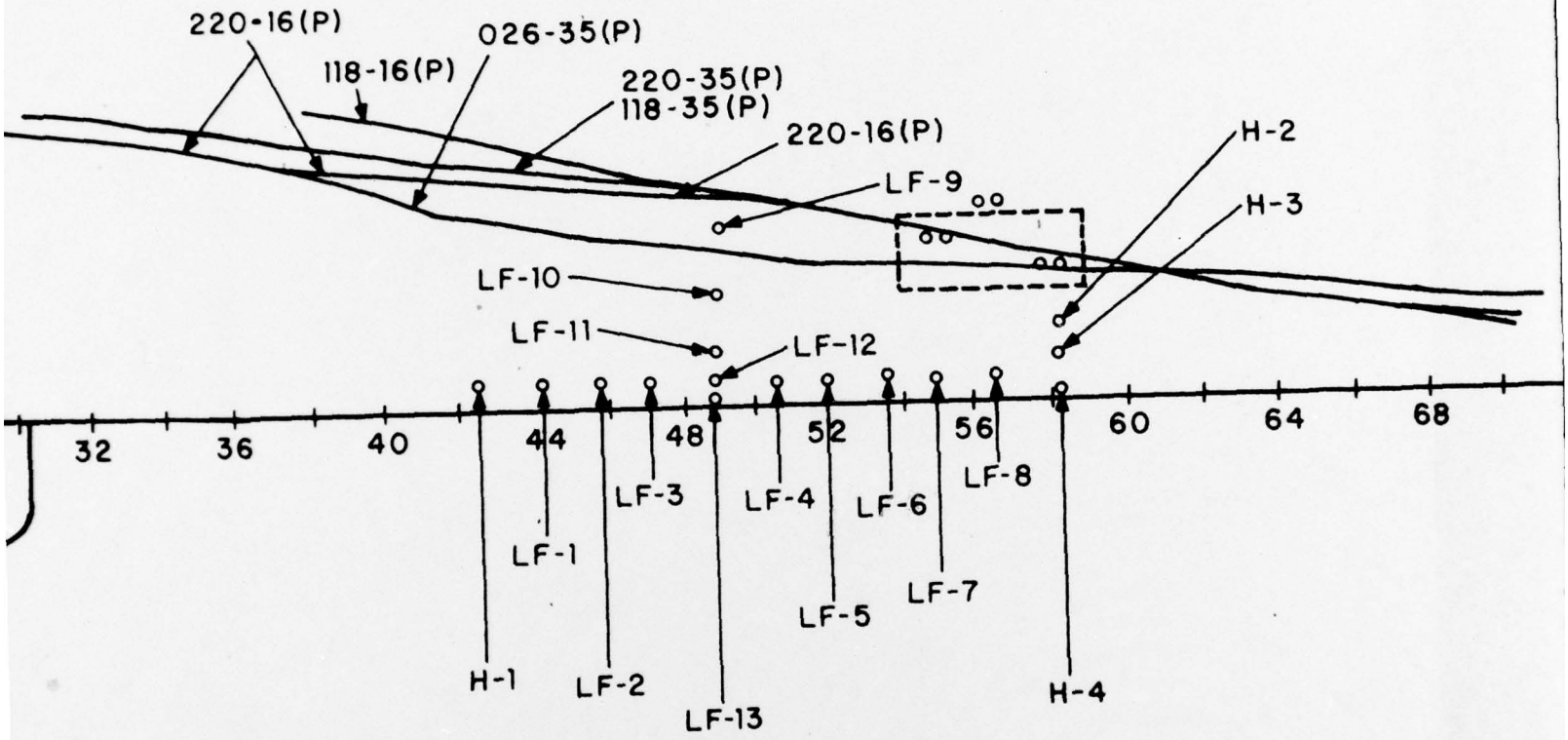

RAL

PURVIS II. 30

8

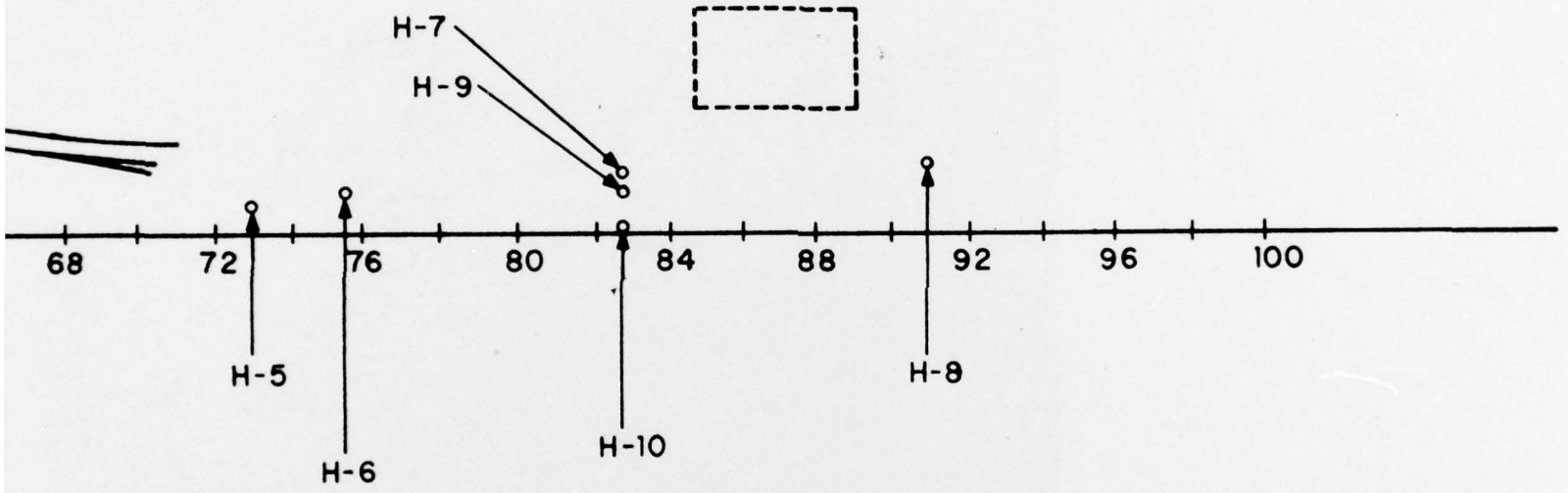

S II. 30 KNOTS-HEAD & FOLLOWING SEA RUNS ONLY

4010

G-5

G-5

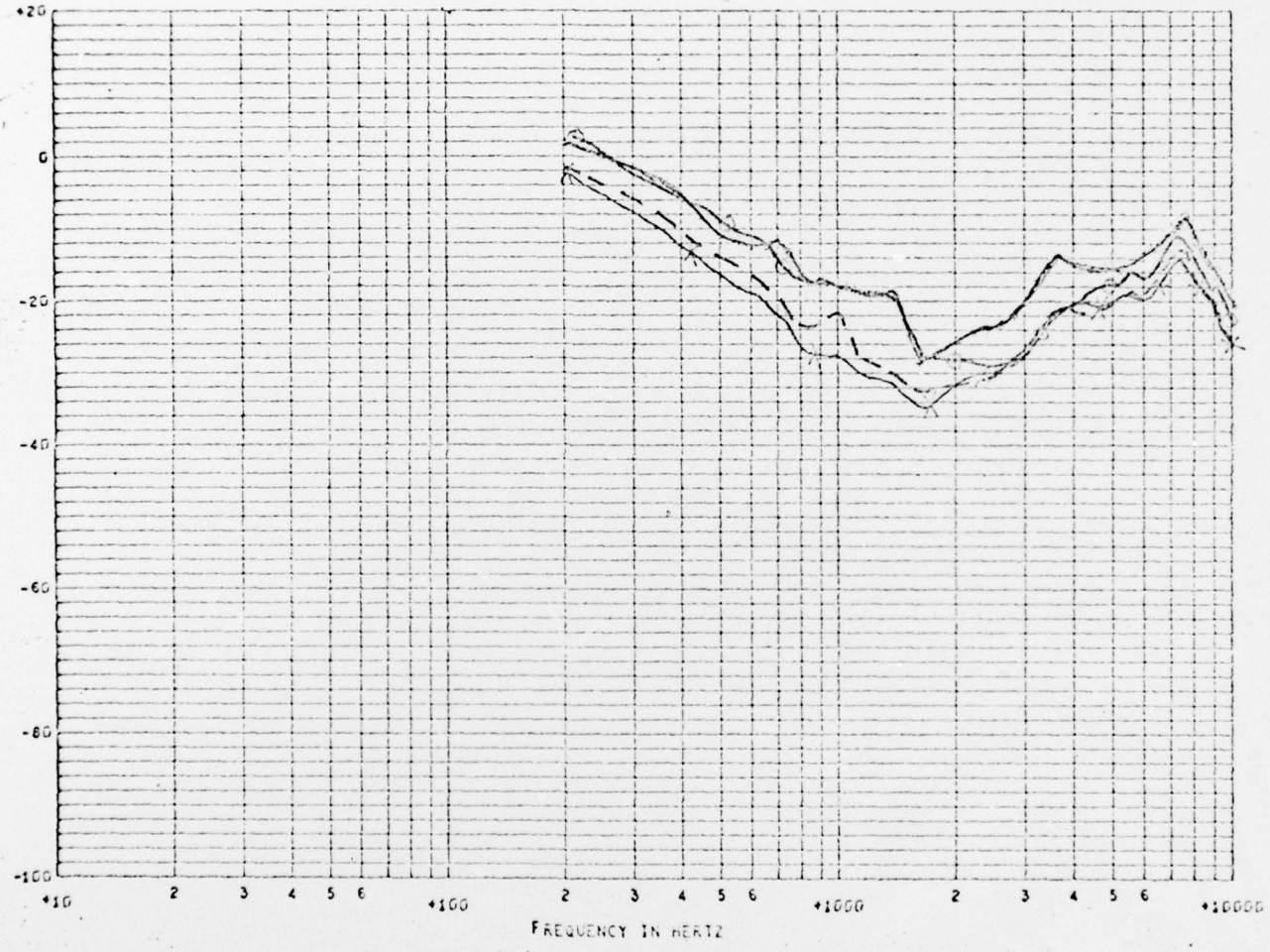

SPECTRUM DB REF 1 MICROBAR SQUARED TIMES SEC OXX LOW BAND CF209 - 35A HI BAND CF209 - 38A
RUN 347A START TIME 16:40:30.0 SPEED 20 HEADING 000 W.R.T. SEA SEA STATE 0

TYPE	SER NO	COMMENTS
HYDRO	G-5	SEA CH 2 093 11.25 00000

Run 347A, 20 KTS ————

Run 347B, 20 KTS —o—o—

Run 340A, 20 KTS —x—x—

Run 340B, 20 KTS - - - -

Fig. 3-8

ELEMENT: G-8

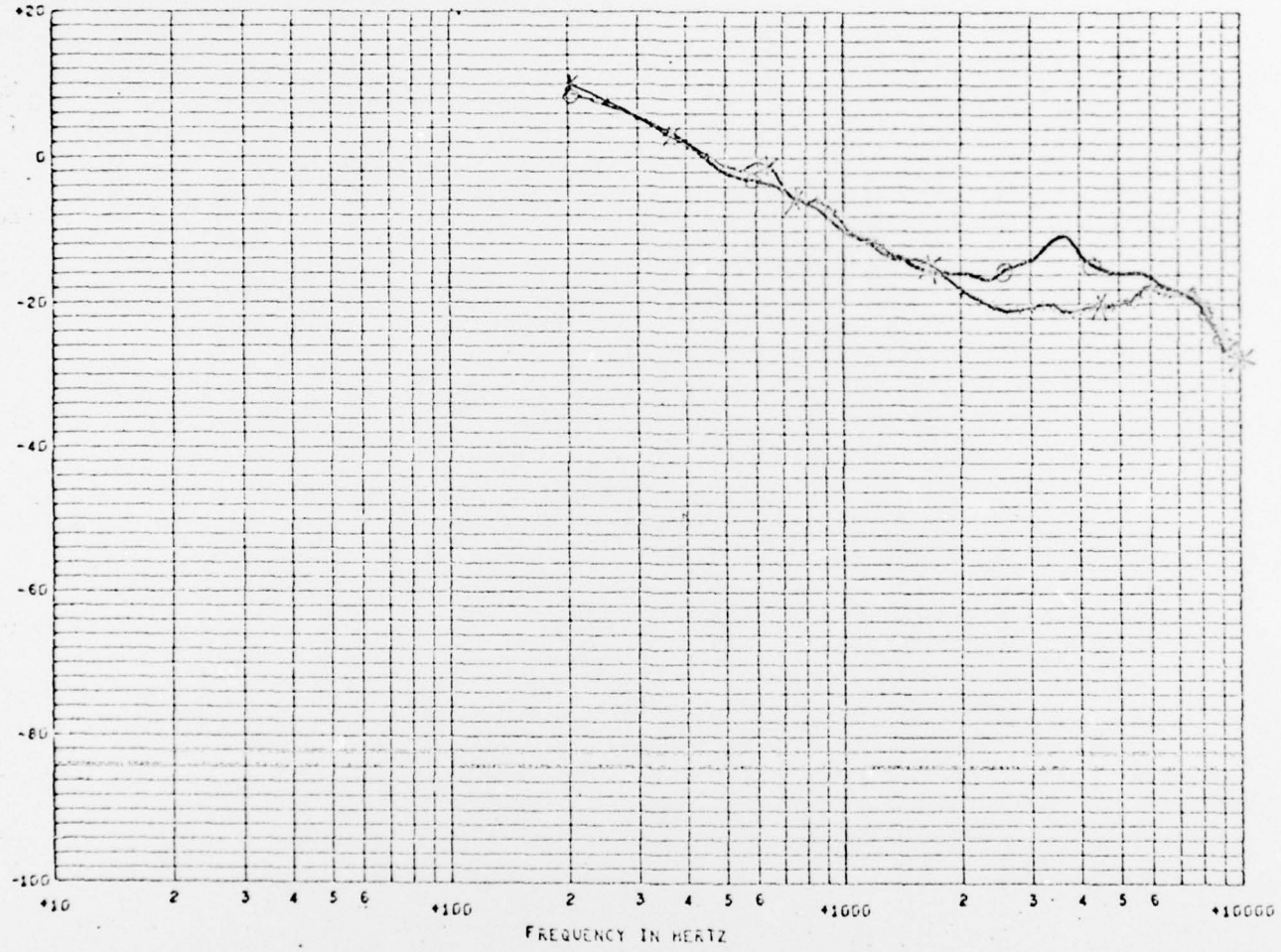

SPECTRUM DB REF 1 MICROBAR SQUARED TIMES SEC GXX LOW BAND CF209 - 49B HI BAND CF209 - 52B
RUN 347D START TIME 11449+58.0 SPEED 20 HEADING 000 W.R.T. SEA SEA STATE 1

TYPE	SER NO	COMMENTS
HYDRO	G-8	SEA CH 2 099 07.75 00000

Run 347A, 20 KTS, —o—o—

Run 347B, 20 KTS, —x—x—

Fig. 3-7

CONFIDENTIAL

1093

ELEMENT G-5

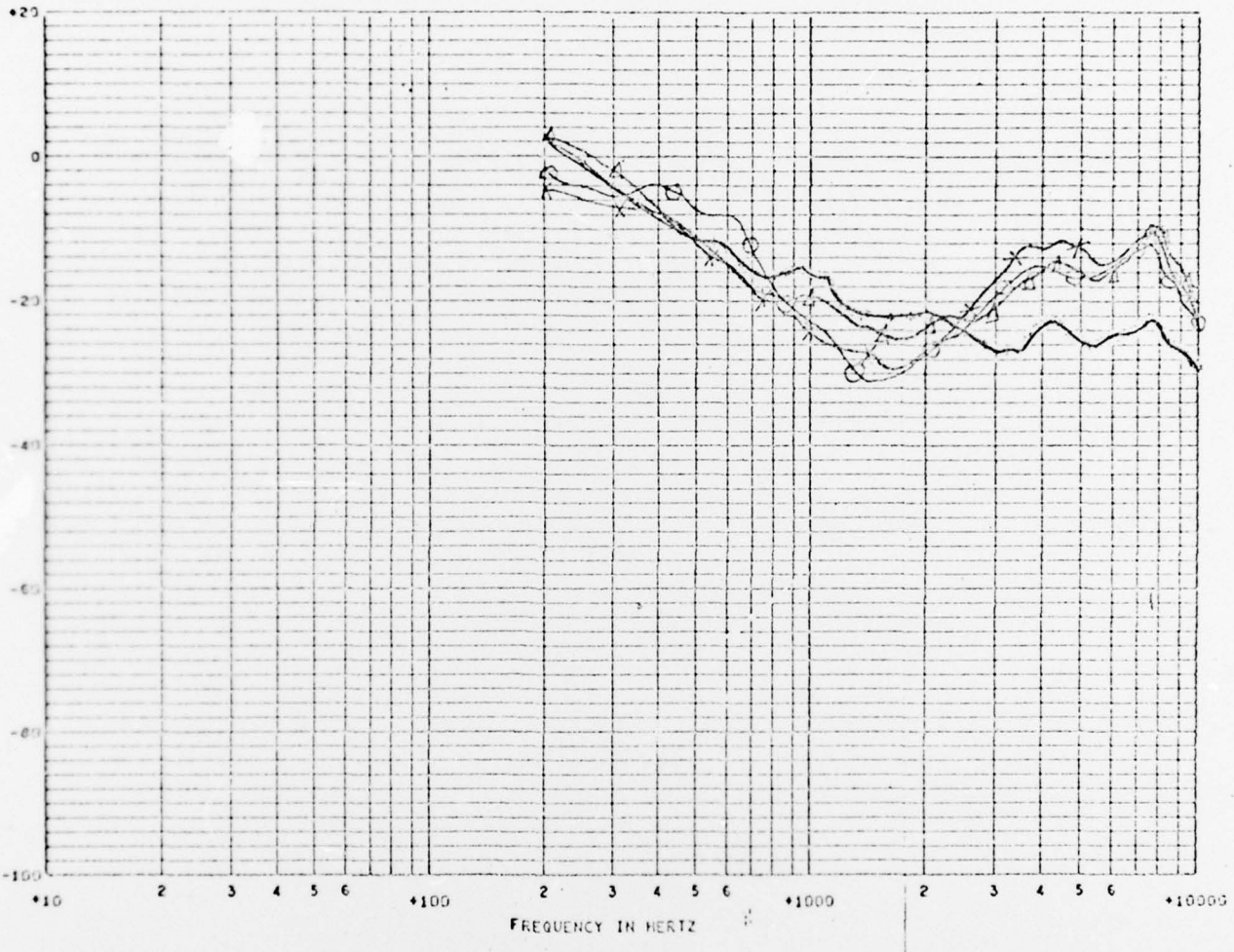

SPECTRUM DB REF 1 MICRODAR SQUARED TIMES SEC 0XX LOW BAND CF100 - 79A - HIGH BAND CF100 - 81A
RUN 348A START TIME 12405930.0 SPEED 25 HEADING 000

TYPE	SER NO	FT FROM BOW
TRG	G-5	093 11.25

15 KTS, 0°, Run 346A

15 KTS, 90°, Run 442

25 KTS, 0°, Run 348

25 KTS, 90°, Run 444

CONFIDENTIAL

Fig. 3-10

1699

ELEMENT: G-8

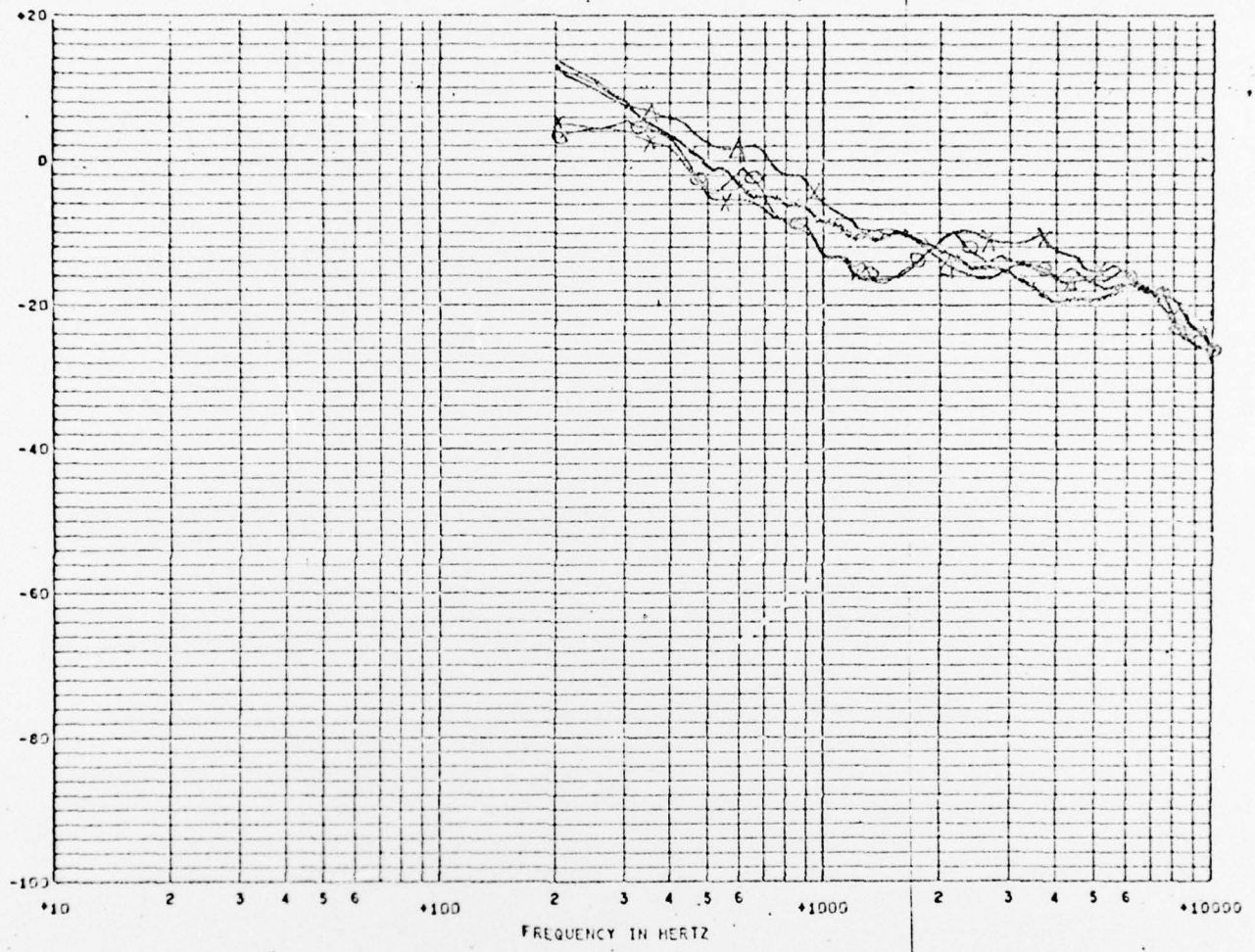

SPECTRUM DB REF 1 MICROBAR SQUARED TIMES SEC GXX LOW BAND CF100 - 80A - HIGH BAND CF100 - 82A
RUN 348A START TIME 12405430.0 SPEED 25 HEADING 000
TYPE SER NO FT FROM BOW
TRC G-8 099 07.75

15 KTS, 0°; Run 346A
15 KTS, 90°; Run 442
25 KTS, 0°; Run 348A
25 KTS, 90°; Run 444

Fig. 3-11

1149

ELEMENT: D1H

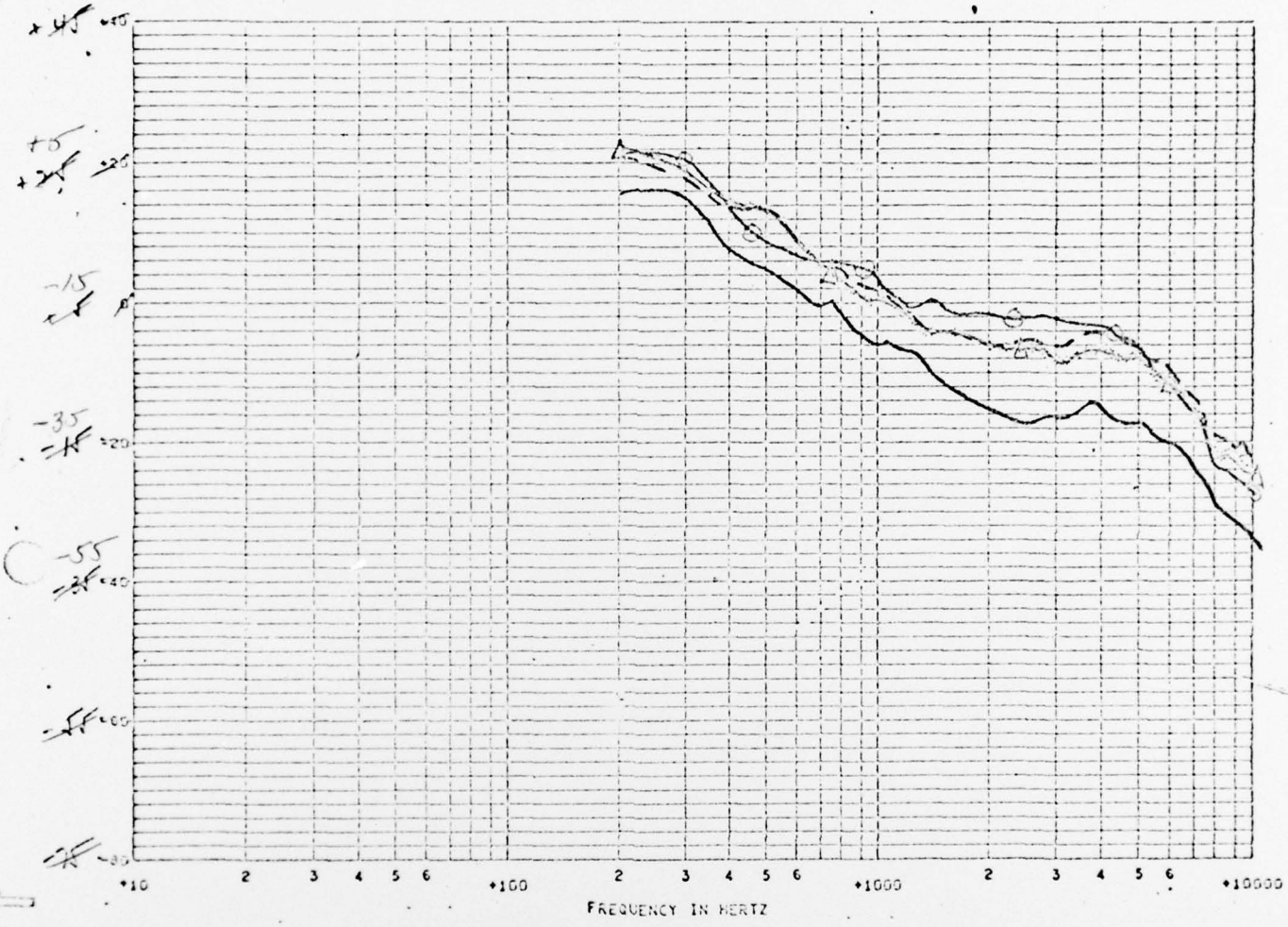

SPECTRUM DD REF 1 MICROBAR SQUARED TIMES SEC GXX LOW BAND CF100 - 60A - HIGH BAND CF100 - 58A
RUN 341A START TIME 11458900.0 SPEED 25 HEADING 000
TYPE SER NO FT FROM DOW
TRG •DBM D1H

15 KTS, 0°, RUN 339A
15 KTS, 90°, RUN 435
25 KTS, 0°, RUN 341A
25 KTS, 90°, RUN 437

FIG. 3-12

4097

ELEMENT: D2H

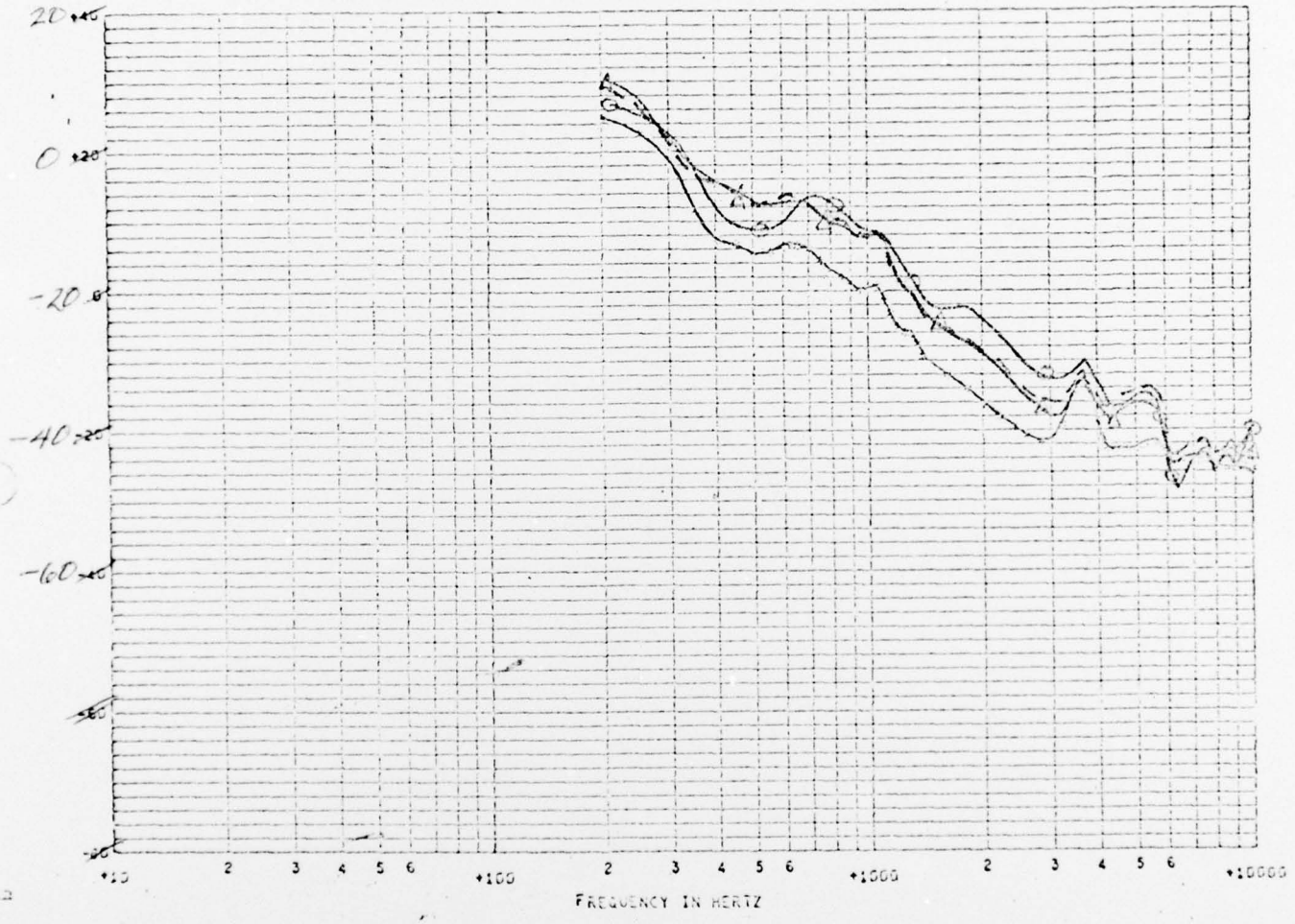

SPECTRUM DB REF 1 MICROBAR SQUARED TIMES SEC 0XX LOW BAND CP17 - 40A HI BAND CP17 - 47A
RUN 339A START TIME 16:21:10.0 SPEED 15 HEADING 000 W.R.T. SEA SEA STATE 0

TYPE	SER NO	COMMENTS
HYDRO	D2H	SEA CH 1

A: 15 KTS, 0°, RUN 339A ——————

B: 15 KTS, 90°, RUN 435 —o——o—

C: 25 KTS, 0°, RUN 341A —Δ——Δ—

D: 25 KTS, 90°, RUN 437 — — — — —

FIG. 3-13

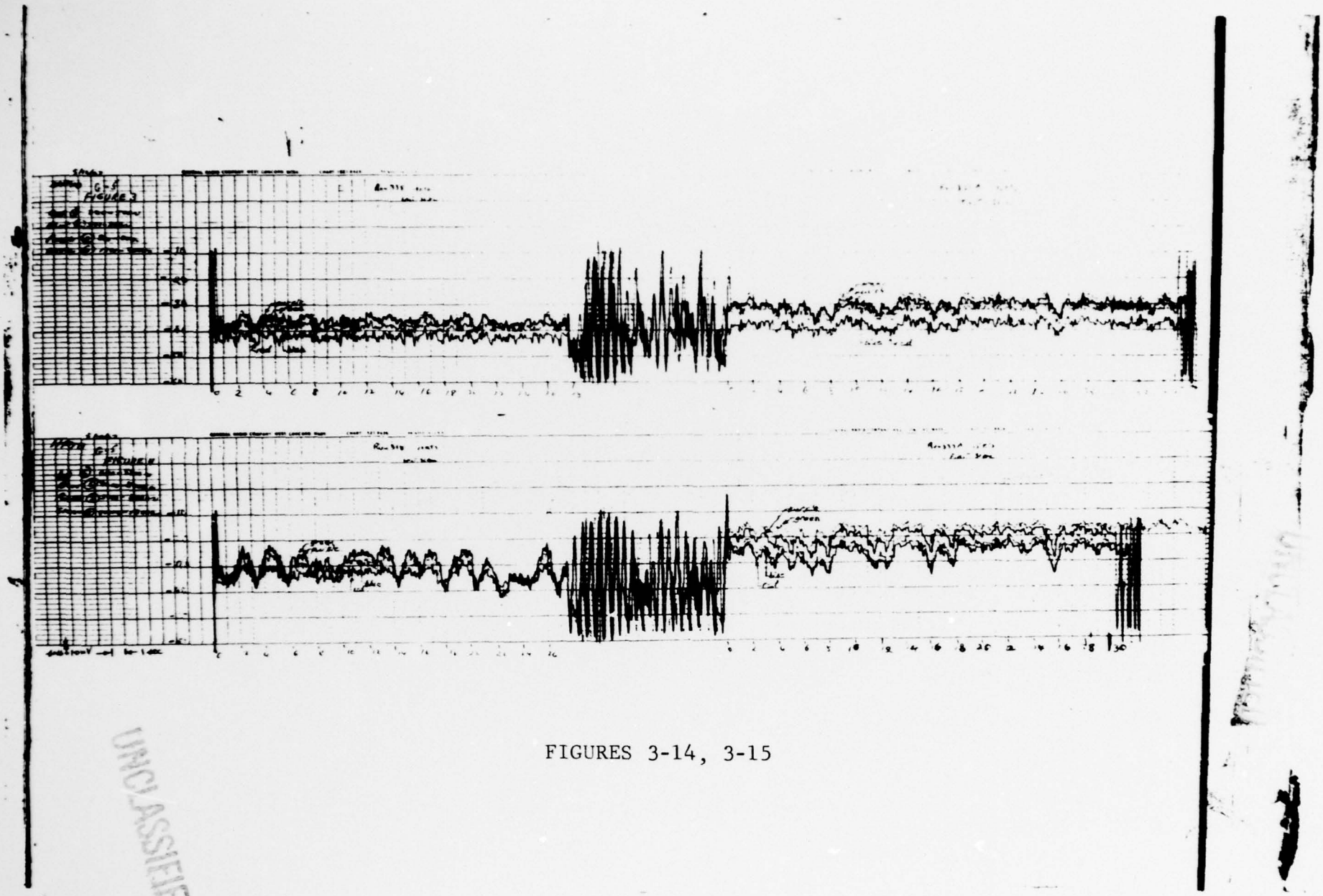

FIGURES 3-14, 3-15

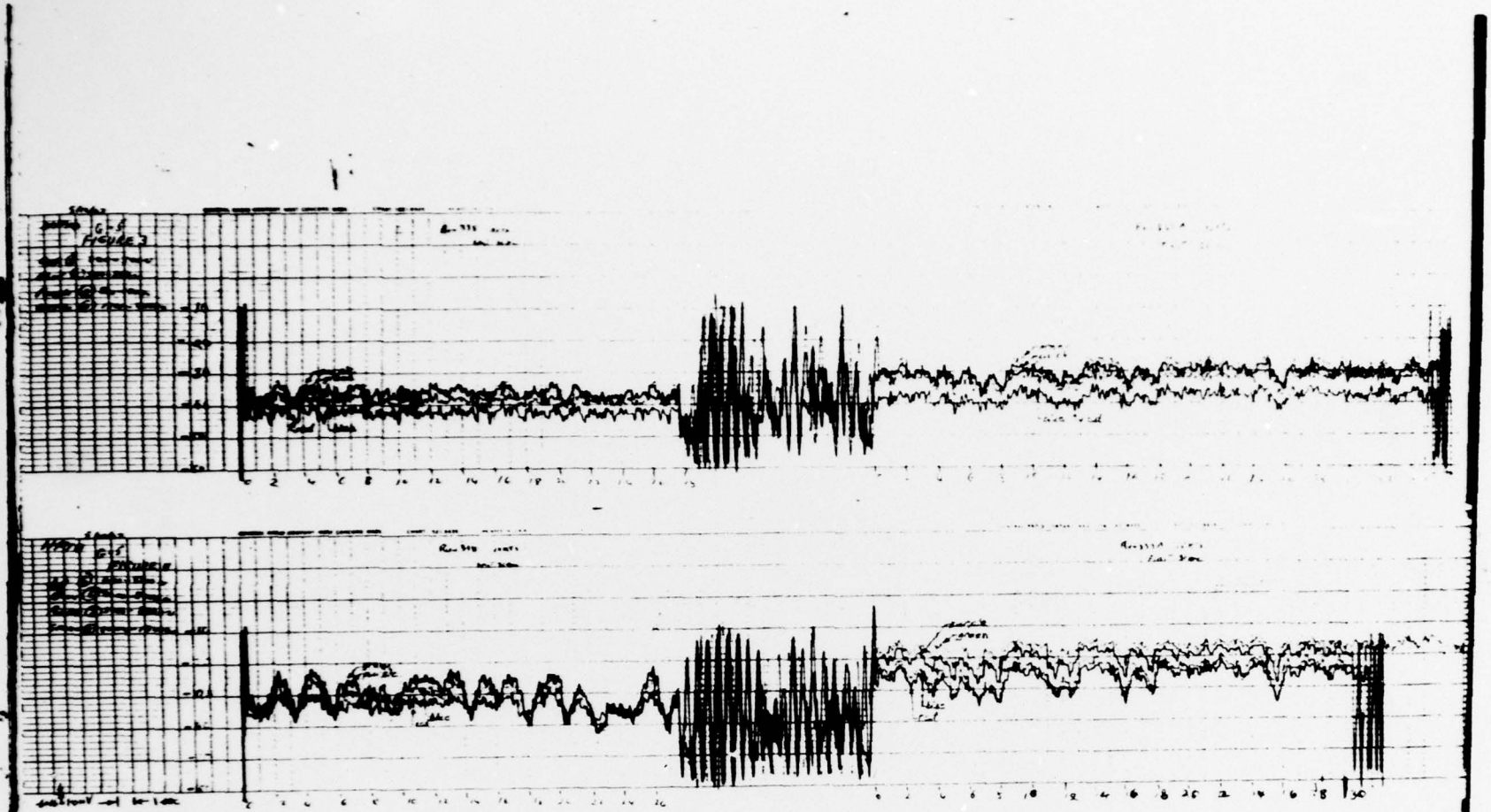

FIGURES 3-16, 3-17

UNCLASSIFIED